HIGH-EFFICIENCY AMORPHOUS SILICON ALLOY BASED SOLAR CELLS AND MODULES

Annual Technical Progress Report
May 30, 2002 through May 31, 2003

S. Guha and J. Yang
United Solar Systems Corp.
Troy, Michigan

NREL Technical Monitor: Bolko von Roedern

Prepared under Subcontract No. ZDJ-2-30630-19

Preface

This annual Subcontract Report covers the work performed by United Solar Systems Corporation for the period from May 30, 2002 to May 31, 2003 under NREL thin film partnership Subcontract No. ZDJ-2-30630-19. The following personnel participated in this research program.

A. Banerjee, E. Chen, G. Fischer, S. Guha (Principal Investigator), M. Hopson, N. Jackett, K. Lord, A. Mohsin, T. Nazmee, J. Noch, T. Palmer, G. Pietka, D. Wolf, B. Yan, J. Yang (Co-Principal investigator), K. Younan, and G. Yue.

Collaboration with the Colorado School of Mines, University of North Carolina, University of Oregon, Syracuse University, and the National Renewable Energy Laboratory is acknowledged. We would like to thank S. Sundquist for preparation of this report.

Executive Summary

Objectives

The principal objective of this R&D program is to expand, enhance, and accelerate knowledge and capabilities for development of high efficiency hydrogenated amorphous silicon (a-Si:H) and amorphous silicon-germanium alloy (a-SiGe:H) related thin film multi-junction solar cells and modules with low manufacturing cost and high reliability. Our strategy has been to use the spectrum-splitting triple-junction structure, a-Si:H/a-SiGe:H/a-SiGe:H, to improve solar cell and module efficiency, stability, and throughput of production. The methodology used to achieve the objectives was: i) explore the highest stable efficiency using the triple-junction structure deposited using RF glow discharge at a low rate, ii) fabricate the devices at a high deposition rate for high throughput and low cost, and iii) develop optimized recipe using the R&D batch large-area reactor to help the design of the production roll-to-roll machines. In the last few years, research on microcrystalline silicon (μc-Si:H) solar cells has attracted significant attention in Japan and Europe. Using μc-Si:H as the bottom cell in multi-junction structures, cell efficiency over 14% and module efficiency over 13% have been reported. We have been exploring the use of μc-Si:H as an intrinsic layer of the bottom cell in the triple-junction solar cell to achieve higher stable cell and module efficiency. During the past year, we have worked on developing high efficiency μc-Si:H single-junction solar cell and high efficiency multi-junction solar cells based on μc-Si:H as the intrinsic layer of the bottom cell.

Approach

In manufacturing, United Solar uses a triple-junction spectral-splitting solar cell structure fabricated using a roll-to-roll technology. The conventional a-Si:H/a-SiGe:H/a-SiGe:H triple-junction cells uses a-Si:H top cell (~1.8 eV bandgap) to absorb the blue light, a-SiGe:H middle cell with ~20% germanium (~1.6 eV bandgap) to absorb the green light, and a-SiGe:H bottom cell with ~40% germanium (~1.4 eV bandgap) to capture the red light. One objective of this program is to develop microcrystalline silicon (μc-Si:H) solar cell as a potential replacement of the a-SiGe:H bottom cell in the triple-junction structure. In the first year, we worked on the development of μc-Si:H single-junction and a-Si:H/μc-Si:H double-junction cells. Another objective is to work on large area deposition issues using the a-Si:H/a-SiGe:H/a-SiGe:H triple-junction structure. For this, we modified the "2B" machine (this is a multichamber R&D deposition machine that can use substrates of area 15" x 14") by replacing the existing deposition cathodes with new fountain cathodes in order to improve the uniformity and cell efficiency. The fountain cathode design is similar to that used in our current 30 MW/year production machine. Any gain in cell efficiency obtained in the 2B machine can be transferred to the production equipment.

In order to accomplish the above objectives, we carried out research in the following areas: i) deposition of μc-Si:H films and solar cells using RF glow discharge at a low rate ~1 Å/s, ii) deposition of μc-Si:H films and solar cells using MVHF glow discharge at a high rate ~3-10 Å/s, iii) metastability of a-Si:H/μc-Si:H double-junction solar cells, iv) metastability of mixed-phase cells containing amorphous and microcrystalline components in the intrinsic layer, and v)

design, fabrication, and installation of new "fountain cathodes" in the 2B machine to simulate the 30 MW/year roll-to-roll production line. In addition, we collaborated with the Colorado School of Mines, University of North Carolina, University of Oregon, Syracuse University, and NREL on material and solar cell characterization and solar cell deposition.

Status/Accomplishments

Small-area cells deposited using RF glow discharge at a low rate

We have worked on developing and optimizing μc-Si:H material and solar cell using RF glow discharge at low rate to search for the highest efficiency with different cell structures. The highest efficiency values achieved are listed below. We give values for active-area efficiency. The grid loss is typically ~7%, and the total area efficiency is therefore ~7% lower.

- 7.4% initial active-area (0.25 cm^2) cell efficiency in a μc-Si:H single-junction structure.
- 13.0% initial and 11.4% stable active-area (0.25 cm^2) cell efficiency in an a-Si:H/μc-Si:H double-junction structure.
- 12.1% initial active-area (0.25 cm^2) cell efficiency in an a-Si:H/a-SiGe:H/μc-Si:H triple-junction structure.

Small-area cells deposited using MVHF glow discharge at high rates

We have used MVHF glow discharge to deposit μc-Si:H material and solar cell at high deposition rates ~ 3-10 Å/s to develop suitable recipes that satisfy production requirements. We have achieved the following results with various deposition times.

- An initial active-area (0.25 cm^2) efficiency of 7.1% has been achieved using a μc-Si:H single-junction cell with 50 minutes of intrinsic layer deposition time.
- An initial active-area (0.25 cm^2) efficiency of 12.3% has been achieved using an a-Si:H/μc-Si:H double-junction cell with 50 minutes of bottom cell intrinsic layer deposition time.
- An initial active-area (0.25 cm^2) efficiency of 11.2% has been achieved using an a-Si:H/μc-Si:H double-junction cell with 30 minutes of bottom cell intrinsic layer deposition time. This cell showed a stable active-area efficiency of 10.4%.

Modification of large-area 2B machine and deposition of solar cells using the constraints of the 30 MW/year production line

- New cathodes with a structure similar to the 30 MW/year machine have been designed, fabricated, and installed in the 2B machine.
- Uniformity of films deposited using the new cathode has been studied. The results showed an improved uniformity.
- a-Si:H and a-SiGe:H alloy component cells have been deposited under the allowable deposition parameters of the 30 MW/year machine.

Stability of a-Si:H/μc-Si:H double-junction solar cells

- We have studied the stability of a-Si:H/μc-Si:H double-junction solar cells under light soaking. We find that a bottom cell limited current mismatch is desirable for stable efficiency.

Light-induced V_{oc} increase in mixed-phase solar cells

- A comprehensive explanation for the light-induced V_{oc} increase in the mixed-phase solar cells has been proposed based on a two-diode equivalent circuit model. This model is consistent with most existing experimental results.
- New experimental results with different a-Si:H buffer layer between the *p* and *i* layers support the two-diode equivalent circuit model.
- Kinetics of light-induced open-circuit voltage (V_{oc}) has been carried out that has provided insight into the mechanism of the light-induced V_{oc} increase. The kinetic results are explained using the two-diode equivalent circuit model.

Publications

1. "Photoinduced stress in hydrogenated amorphous silicon films," E. Stratakis, E. Spanakis, P. Tzanetakis, H. Fritzsche, S. Guha, and J. Yang, Appl. Phys. Lett. **80**, 1734 (2002).
2. "Hydrogenated microcrystalline silicon solar cells made with modified very-high-frequency glow discharge," B. Yan, K. Lord, J. Yang, S. Guha, J. Smeets, and J-M. Jacquet, *Mat. Res. Soc. Symp.*, **715**, pp. 629 – 634 (2002).
3. "Correlation of light-induced enhancement of open-circuit voltage and structural change of heterogeneous silicon solar cells," J. Yang, K. Lord, B. Yan, A. Banerjee, S. Guha, D. Han, and K. Wang, *Mat. Res. Soc. Symp.*, **715**, pp. 601 - 610 (INVITED) (2002).
4. "Ultralight amorphous silicon alloy photovoltaic modules for space applications," K. J. Beernink, G. Pietka, J. Noch, K. Younan, D. Wolf, A. Banerjee, J. Yang, and S. Guha, *Mat. Res. Soc. Symp.*, V6.3 (2002).
5. "Correlation of the open-circuit voltage enhancement of heterogeneous silicon solar cells and the Staebler-Wronski effect," J. Yang, K. Lord, B. Yan, A. Banerjee, and S. Guha, *29th IEEE PVSC*, pp. 1094 - 1097 (2002).
6. "Amorphous silicon alloy materials, cells, and modules," S. Guha and J. Yang, *29th IEEE PVSC*, pp. 1070 - 1075 (2002).
7. "Short-range compositional randomness of hydrogenated amorphous silicon-germanium films," B. D. Chapman, S. W. Han, G. T. Seidler, E. A. Stern, J. D. Cohen, S. Guha, and J. Yang, *J. Appl. Phys.*, **92**, 801 (2002).
8. "Wide-gap thin film Si *n-i-p* solar cells deposited by hot-wire CVD," Q. Wang, E. Iwaniczko, J. Yang, K. Lord, S. Guha, K. Wang, and D. Han, *29th IEEE PVSC*, pp. 1222 – 1225 (2002).
9. "Nonuniform H distribution in thin-film hydrogenated amorphous Si by small-angle neutron scattering," D. L. Williamson, D. W. M. Marr, J. Yang, B. Yan, and S. Guha, Phys. Rev. B **67**, 075314 (2002).

10. "Status of hydrogenated microcrystalline silicon solar cells at United Solar," J. Yang, B. Yan, G. Yue, A. Banerjee, K. Lord, and S. Guha, NCPV and Solar Program Review Meeting, Denver, March 24 – 26, 2003.
11. "Micro-Raman measurements of mixed-phase hydrogenated silicon solar cells," J. Owens, D. Han, B. Yan, J. Yang, K. Lord, and S. Guha, NCPV and Solar Program Review Meeting, Denver, March 24 – 26, 2003.
12. "Amorphous and thin-film silicon," B. Nelson, H. Atwater, B. von Roedern, J. Yang, P. Sims, X. Deng, V. Dalal, D. Carlson, and T. Wang, NCPV and Solar Program Review Meeting, Denver, March 24 – 26, 2003.
13. "Correlation of material properties and open-circuit voltage of amorphous silicon based solar cells," B. Yan, J. Yang, G. Yue, and S. Guha, MRS Spring Meeting, San Francisco, April 21 – 25, 2003.
14. "Hydrogenated microcrystalline silicon single-junction and multi-junction solar cells," B. Yan, G. Yue, J. Yang, A. Banerjee, and S. Guha, MRS Spring Meeting, San Francisco, April 21 – 25, 2003.
15. "Kinetics of light-induced effects in mixed-phase hydrogenated silicon solar cells," G. Yue, B. Yan, J. Yang, K. Lord, and S. Guha, MRS Spring Meeting, San Francisco, April 21 – 25, 2003.
16. "Bandtail limits to solar conversion efficiencies in amorphous silicon solar cells," K. Zhu, J. Yang, W. Wang. E. Schiff, J. Liang, and S. Guha, MRS Spring Meeting, San Francisco, April 21 – 25, 2003.
17. "Micro-Raman studies of mixed-phase hydrogenated silicon solar cells," J. Owens, D. Han, B. Yan, J. Yang, K. Lord, and S. Guha, MRS Spring Meeting, San Francisco, April 21 – 25, 2003.
18. "Deposition of device quality μc-Si films and solar cells at high rates by HWCVD in a W filament regime where W/Si formation is minimal," E. Iwaniczko, A. H. Mahan, B. Yan, L. N. Gedvilas, D. L. Williamson, and B. P. Nelson, MRS Spring Meeting, San Francisco, April 21 – 25, 2003.
19. "Microcrystalline silicon solar cells made using RF, MVHF, and microwave at various deposition rates," B. Yan, G. Yue, J. Yang, K. Lord, A. Banerjee, and S. Guha, WCPEC-3 (World Conference on Photovoltaic Energy Conversion), Osaka, May 11 – 18, 2003. (INVITED)
20. "On the mechanism of light-induced open-circuit voltage increase in mixed-phase hydrogenated silicon solar cells," B. Yan, J. Yang, G. Yue, K. Lord, and S. Guha, WCPEC-3 (World Conference on Photovoltaic Energy Conversion), Osaka, May 11 – 18, 2003.
21. "Roll-to-roll production of amorphous silicon based triple junction solar cells," S. Guha, WCPEC-3 (World Conference on Photovoltaic Energy Conversion), Osaka, May 11-18, 2003. (INVITED)
22. "Effect of hydrogen dilution on the open-circuit voltage of hydrogenated amorphous silicon solar cells," B. Yan, J. Yang, and S. Guha, accepted by Appl. Phys. Lett., (2003).
23. "On light-induced increase in open-circuit voltage of mixed-phase hydrogenated silicon solar cells," B. Yan, G. Yue, J. Yang, K. Lord, and S. Guha, submitted to Appl. Phys. Lett., (2003).

Section 1

Introduction

United Solar Systems Corp. (United Solar) has achieved world record stable cell efficiency of 13% and module efficiency of 10.5% using a-Si:H/a-SiGe:H/a-SiGe:H triple-junction structure. This technology has been successfully transferred to mass production with a 5 MW/year capability in 1997. In order to expand our production capability, we designed and constructed a new 30 MW/year plant at Auburn Hills, Michigan. The new machine has been producing since early 2003. The main objective of the current R&D research program is to address the Department of Energy (DoE) goal of attaining 15% thin film module efficiency by developing new materials, device designs, and inexpensive manufacturing processes. In the past, we worked on a-Si:H and a-SiGe:H alloy based solar cells. The a-Si:H/a-SiGe:H/a-SiGe:H triple-junction structure is currently the frontrunner for obtaining the highest stable cell efficiency. In recent time, μc-Si:H solar cell has emerged as a potential substitute for the middle and bottom cells in the multijunction structure due to no light-induced degradation and no GeH_4 needed in the deposition process. Kaneka Corp. has reported over 14% initial cell efficiency using a-Si:H/μc-Si:H double-junction structure and Canon Inc. achieved over 13% initial a-Si:H/μc-Si:H/μc-Si:H triple-junction module efficiency.

United Solar has also started work on the development of μc-Si:H solar cells with the objective of using the μc-Si:H layer as the intrinsic layer in a multi-junction structure. We have carried out the deposition of μc-Si:H materials and solar cells using conventional RF glow discharge at a low rate ~1 Å/s to explore the practical limits of achievable efficiency. Concurrently, we have worked on the modified VHF (MVHF) technique at high deposition rates ~3-10 Å/s to develop the technology that is compatible with production. In a parallel effort, we have also worked on large area deposition issues that impact the success of the 30 MW/year. For this purpose, we redesigned new fountain cathodes for the 2B machine taking into account the constraints of the production machine. The new hardware has been fabricated and installed in the machine and uniformity studies have been carried out. Preliminary component cell results have been obtained. Further optimization of the process parameters is under way.

μc-Si:H solar cell has been reported to exhibit no light-induced degradation. However, in a multi-junction structure, the top cell is usually an a-Si:H cell with relatively thick intrinsic layer to generate enough current for current matching with the μc-Si:H bottom cell. A thick a-Si:H cell might lead to a poor overall stability. Therefore, the stability study of a-Si:H/μc-Si:H double-junction will provide useful feedback for cell design in order to achieve high stable efficiency. We have carried out light-soaking studies for a-Si:H/μc-Si:H double-junction cells deposited at various deposition rates. In the past, we have reported light-induced V_{oc} increase in mixed-phase solar cells, a phenomenon different from conventional a-Si:H solar cell. In this year, we continued to search the mechanism of the light-induced V_{oc} increase.

Section 2

Microcrystalline Silicon Cells Deposited Using Conventional RF Glow Discharge

2.1. Experimental

A multi-chamber RF system (named Line System) has been used to deposit a-Si:H and μc-Si:H materials and solar cells. The a-Si:H top cell was deposited on specular stainless steel substrate. The component μc-Si:H bottom cell was deposited on stainless steel, and on Al/ZnO or AgZnO back reflector to enhance the long-wavelength absorption. ITO dots with an active-area of 0.25 cm^2 were deposited on the *p* layer and grid fingers were deposited for the top contact. The solar cell performance was measured under an AM1.5 solar simulator at 25 °C with quantum efficiency correction for short-circuit current density. In order to check the individual cell performance in the double-junction structure, the light J-V characteristics were measured under an AM1.5 solar simulator with a 610 nm cut-on filter and a 585 nm cut-off filter.

The material properties of μc-Si:H films and solar cells have been characterized by photoluminescence, Raman spectroscopy (at University of North Carolina), X-ray diffraction and small angle X-ray diffraction (at the Colorado School of Mines). These results will be reported separately by Daxing Han and Don Williamson. These characterizations provide useful information for understanding the material properties and their correlation to cell performance. The device properties were also characterized by dark current-voltage (J-V) measurement at different temperatures.

2.2. Light-trapping effect

High efficiency solar cells require not only high quality materials but also optimized cell structure. For μc-Si:H solar cells, due to the indirect optical transition in microcrystallites, the absorption coefficients are not high enough to generate high current density with a thickness less than 1 μm. Therefore, an optimized back reflector is very important for increasing cell efficiency by light trapping effect. Figure 1 shows quantum efficiency plots for three solar cells deposited on stainless steel (ss), Al/ZnO back-reflector coated ss, and Ag/ZnO coated ss. It is noted that the solar cells deposited on the back reflectors have significant response in the long wavelength region, especially the cell on Ag/ZnO back reflector. However, the short wavelength response is lower, a phenomenon also observed in a-Si:H and a-SiGe:H solar cells. It is probably due to increased back diffusion of photo-generated electrons near the *p/i* interface of cells deposited on a textured substrate compared to a specular substrate. The low quantum efficiency in the short wavelength region for the cell deposited on back reflector corresponds to low blue FF, as listed in Table I. The slightly higher V_{oc} and lower FF for the cells deposited on back reflector result from the high density of photo-generated carriers. A higher density of photo-generated carriers produces a wider split of quasi-Fermi levels leading to a larger V_{oc}, and a higher recombination rate leads to a lower FF. Since μc-Si:H normally has higher response in the long wavelength range, shifting the minimum reflection point to longer wavelength would be beneficial for improving J_{sc}.

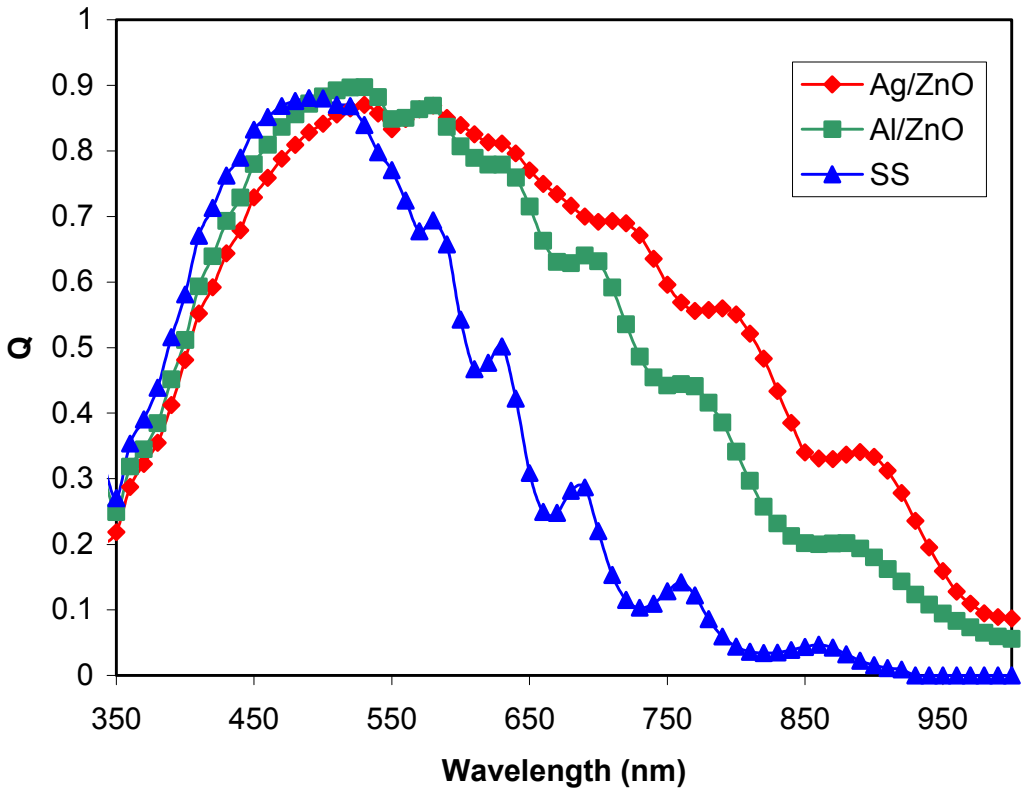

Figure 1. Quantum efficiency of μc-Si:H solar cells made on ss, Al/ZnO coated ss, and Ag/ZnO coated ss substrates.

Table I. J-V characteristics of μc-Si:H solar cells deposited under similar conditions but on different substrates.

Substrate	Efficiency (%)	J_{sc} (mA/cm^2)	V_{oc} (V)	FF	FF_b	FF_r
ss	4.36	13.45	0.478	0.679	0.694	0.698
Al/ZnO/ss	6.45	20.39	0.489	0.647	0.665	0.656
Ag/ZnO/ss	7.25	22.83	0.489	0.649	0.658	0.640

2.3. Thickness dependence of microcrystalline silicon solar cells

The advantages of μc-Si:H cell over a-SiGe:H cells are higher J_{sc} and minimal light-induced degradation. However, some unsolved issues still limit the further improvement of cell efficiency. One big drawback is the lower V_{oc}, which is normally lower than 0.5 V for the cells with high J_{sc} (e.g. > 24 mA/cm^2). In order to improve the cell efficiency further, we need to understand what are the limitations of V_{oc} in μc-Si:H solar cells. For this purpose, we studied the thickness dependence of μc-Si:H single-junction solar cells.

Figure 2 shows the J-V characteristics parameters of the solar cells as a function of intrinsic layer thickness. It was observed that J_{sc} increases, but FF decreases with the increase of intrinsic layer thickness. This phenomenon is similar to that observed in a-Si:H silicon solar cells. For a thicker cell, higher J_{sc} results from higher optical absorption, and lower FF from reduced collection. A significant difference from a-Si:H solar cells is that V_{oc} decreases with intrinsic layer thickness significantly. In a-Si:H solar cells, V_{oc} also decreases with intrinsic layer thickness, but the change is normally very small unless microcrystalline formation occurs. For μc-Si:H cells shown in Fig. 2, V_{oc} decreases with the intrinsic layer thickness dramatically. Although we do not fully understand what causes the thickness dependence of V_{oc} at this moment, we have considered a few possible mechanisms. First, it is known that the amount of microcrystalline inclusion (grain size and crystal volume fraction) increases with film thickness if the deposition conditions remain the same during deposition. We have also found that V_{oc} decreases with an increase of H_2 dilution. Therefore, with increase of microcrystalline portion, V_{oc} varies from over 1.0 V in fully a-Si:H phase to below 0.5 V in substantially microcrystalline phase. The mixed-phase solar cells have V_{oc}'s in between, depending on the amount of crystal volume fraction. Based on the two observations, we conclude that a thicker μc-Si:H cell has a higher average crystal volume fraction, hence, lower V_{oc}. Second, for μc-Si:H cells with an intrinsic layer thickness of around 1 μm, its V_{oc} is normally below 0.5 V, which is much lower than that of single crystalline silicon solar cells. Although we may consider micro-grains to have a similar band gap as crystalline silicon, the distorted bonds in the grain boundary regions lead to an increase in band tail states and cause a lower V_{oc}. In addition, impurity is another issue. We found a significant amount of oxygen impurity in some unoptimized μc-Si:H silicon films. Even for some optimized μc-Si:H films, SIMS analysis showed a large tail diffusing into the film. Oxygen atoms can form n-type doping centers, which move the Fermi level toward the conduction band and lead to a high dark conductivity. In an *nip* structure, a higher dark

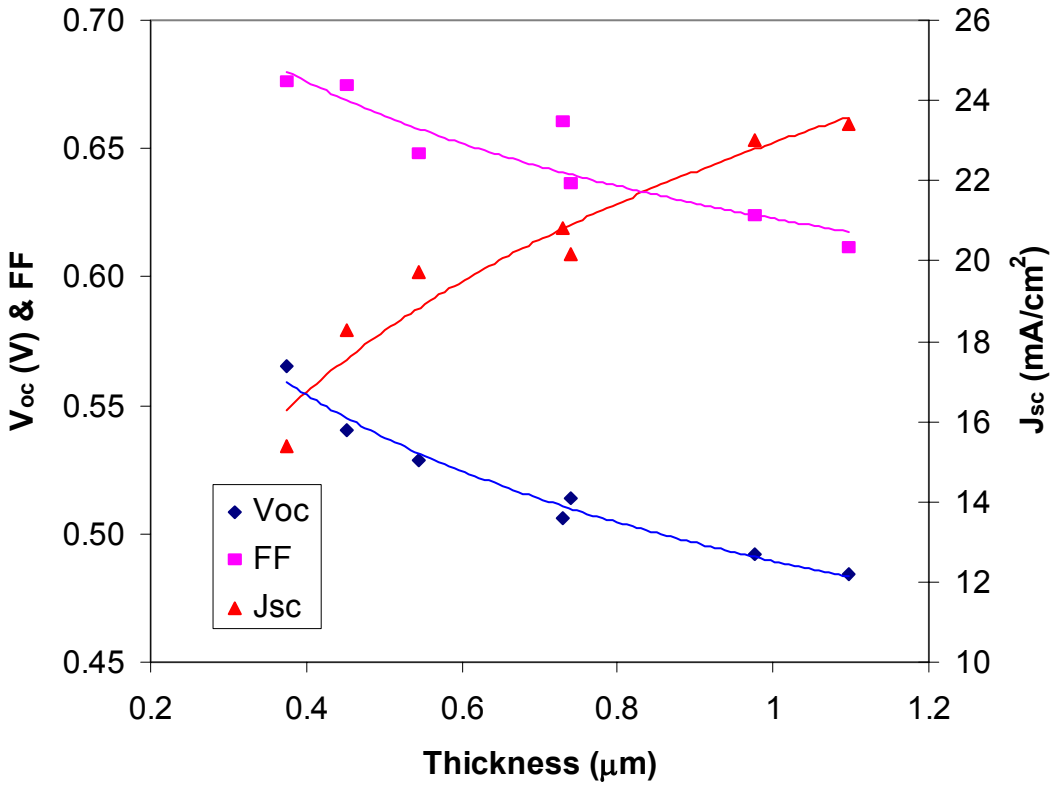

Figure 2. J-V characteristics of μc-Si:H single-junction solar cells versus the intrinsic layer thickness.

conductivity causes higher dark current density and lower V_{oc}. Since we found that the post-deposition impurity diffusion can be blocked by a-Si:H layer, the oxygen problem is not a big issue for multi-junction solar cells, but the incorporation of oxygen during the deposition is still a concern.

Based on the above, it is clear that the challenge is to understand the thickness dependence of cell performance and to fabricate thick μc-Si:H solar cells that yield high J_{sc} without affecting V_{oc} and FF.

2.4. Carrier transport in μc-Si:H solar cells

The carrier transport properties are important for cell performance. Many techniques have been used to measure the carrier transport properties such as carrier mobility and lifetime in μc-Si:H materials. However, most of the techniques require special sample structure or special substrate. However, it has been shown that μc-Si:H material properties depend on cell thickness and substrate, which leads to a question that the obtained transport parameters may not represent the real situation in solar cells. It has been widely accepted that the most reliable material properties should be directly obtained from the device. For this purpose, we carried out dark J-V measurements on real μc-Si:H solar cells.

Figure 3 shows a series of dark J-V characteristics measured at different temperatures for μc-Si:H solar cells deposited on Ag/ZnO back reflector (BR) coated stainless steel substrate and on stainless steel with no back reflector. The interfaces were tailored to reduce the incubation layer and reduce shunt current. The dark J-V curves show perfect diode characteristics over a wide range of temperature as described by the equation:

$$J(V) = J_0\left\{\exp\left(\frac{qV}{nkT}\right) - 1\right\} \qquad (1)$$

where J_0 is the reverse saturation current density, n is the diode quality factor, -q is the charge of an electron, k is the Boltzmann constant, and T is the measurement temperature.

Figure 4 (a) plots J_0 versus 1000/T for two cells deposited using the same recipe but one on ss and the other on Ag/ZnO back reflector coated ss. Both cells show a linear relationship on the semi-log plot and give the same activation energy of 0.65 eV. If the Fermi-level is at the center of the bandgap, twice the value of the activation energy is equal to the electronic bandgap. Since most μc-Si:H materials show weak *n*-type transport, we can conclude that the electronic bandgap in the μc-Si:H intrinsic layer is >1.3 eV. Referring to Fig. 4(a), the curve for the BR cell is shifted by a factor of 3 higher than the ss cell. The shift may be attributed to the larger effective area of the BR cell due to the texture of the back reflector. Figure 4(b) plots n versus T for the same two samples. The decrease of n with the increase of temperature indicates an increased diffusion length (or mobility) at high temperature; the larger n for the cell on Ag/ZnO back reflector is probably due to the larger effective path for carrier transport across the intrinsic layer due to the texture of Ag/ZnO back reflector.

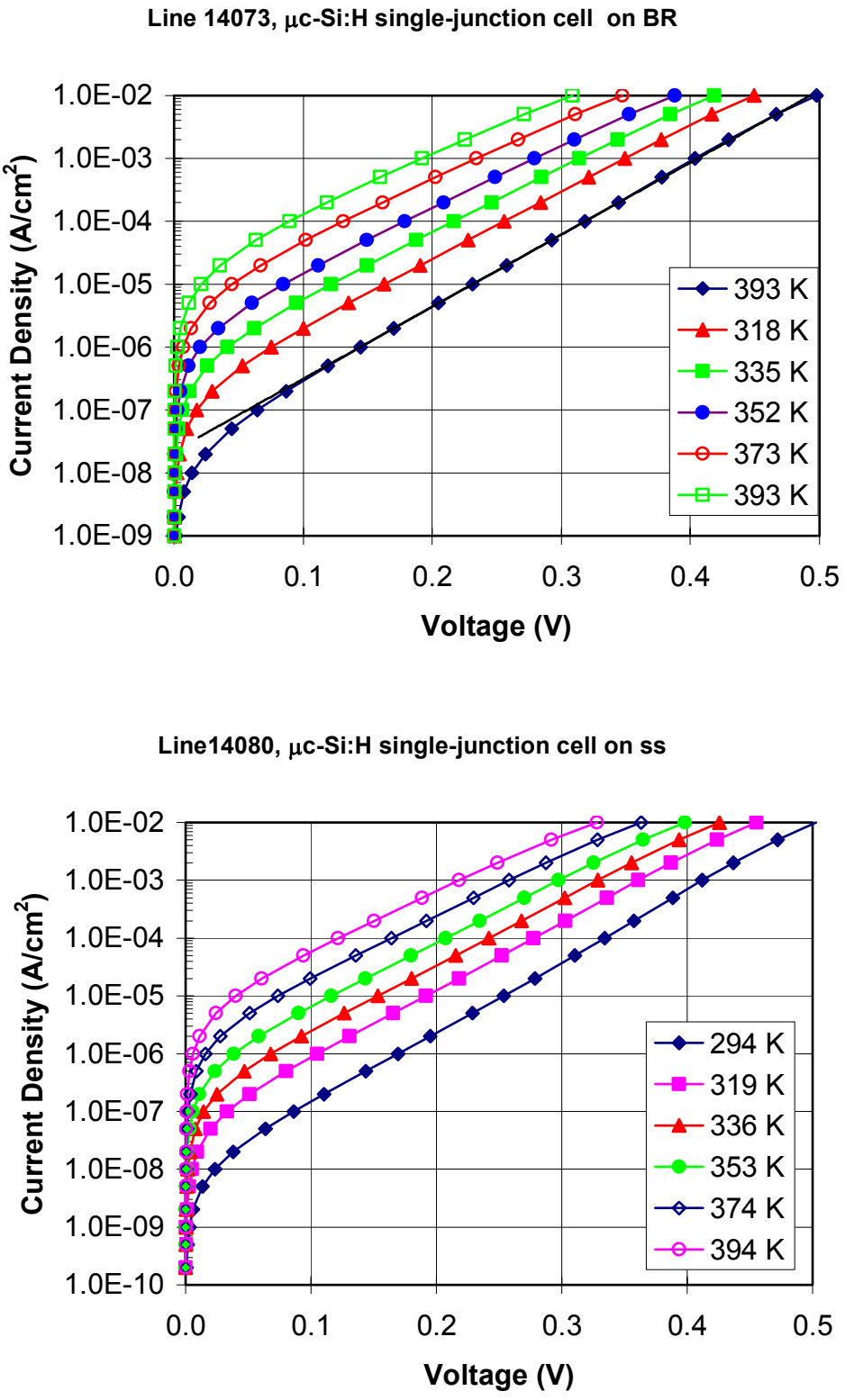

Figure 3. Dark J-V characteristics measured at different temperatures for μc-Si:H solar cells deposited on Ag/ZnO back reflector and on stainless steel.(ss).

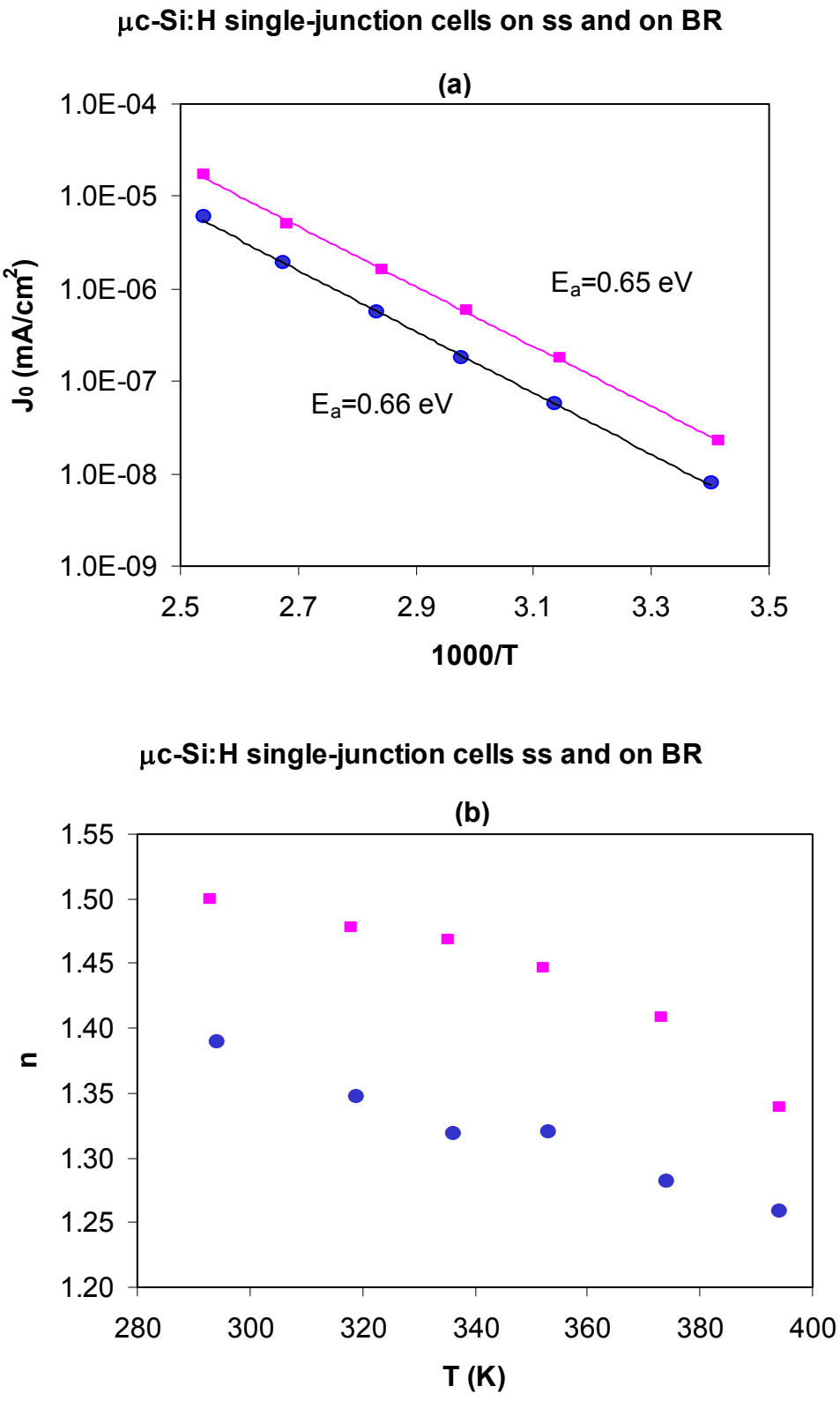

Figure 4. (a) J_0 versus 1000/T and (b) n versus T for μc-Si:H single-junction solar cells made on Ag/ZnO (BR) coated ss (■) and specular ss (●).

2.5. Control of interfaces

High material quality in all the layers of the device is essential, but does not ensure a high solar cell efficiency. Previous studies of a-Si:H and a-SiGe:H solar cells showed that an optimized interface between the intrinsic layer and doped layers is also important. Similarly, for μc-Si:H *nip* solar cells, we need to optimize the material quality for each layer as well as control the interface. Figure 5 shows the light J-V characteristics of solar cells with different interface layers: (a) optimized *n/i* and *i/p* buffer layers, (b) *n/i* buffer layer only, (c) *i/p* buffer layer only, and (d) no *n/i* and *i/p* buffer layers. The four solar cells were made on Ag/ZnO back reflector with the same recipe except different buffer layers at the *n/i* and *i/p* interfaces. The μc-Si:H layer was deposited using RF glow discharge at ~1 Å/s with a thickness ~0.9 μm. Comparing the results of 5(a) and 5(b), we find that without the *i/p* buffer layer, the V_{oc} and FF are lower. The lower V_{oc} may be attributed to the higher shunt current as shown in Fig. 6, where the cell with no *i/p* buffer layer has a significantly higher shunt current at lower bias than the cell with *i/p* buffer layer. The mechanism for the high shunt current is not clear. We believe that the leakage through grain boundary is probably the source of shunt current in μc-Si:H solar cells. Comparing the results of Fig. 5(a) and 5(c), we find that V_{oc} is slightly higher, but J_{sc} and FF are lower for the cell with no *n/i* buffer layer than with *n/i* buffer layer. The higher V_{oc} and lower J_{sc} indicate a lower average microcrystal volume fraction in the intrinsic layer for the sample with no *n/i* buffer layer than with *n/i* buffer layer. The poorer FF with no *n/i* buffer layer may be due to a poorer carrier transport. Normally, there is a crossover between the dark and light J-V curves as shown in Figs. 5(c) and (d); a phenomenon that often appears in mixed-phase solar cells. The crossover is due to a low forward current in the dark as shown in Fig. 6, where the dark J-V levels off from the exponential line at the high voltage for the samples with no *n/i* buffers. The cell with no buffer layer has the lowest efficiency with large crossover between dark and light J-V characteristics, and the dark J-V shows a high shunt current at low bias and levels off at high bias. From this study we conclude that as in the case of a-Si:H and a-SiGe:H alloy solar cells, the interface between the intrinsic μc-Si:H layer and the doped layers are also very important. We continue to work on the optimization of the interface layers.

2.6. Microcrystalline Si single-junction solar cells

In order to obtain high efficiency multi-junction solar cells, it is first necessary to optimize the component cells. In the a-Si:H/a-SiGe:H/μc-Si:H triple-junction structure, we can use essentially the same top and middle component cells as used in the a-Si:H/a-SiGe:H/a-SiGe:H triple-junction structure with only minor adjustments. The major effort was on the development of a high-efficiency μc-Si:H bottom cell. We achieved an initial active-area efficiency of 7.4%. Figure 7 plots the J-V characteristics and quantum efficiency of the best μc-Si single-junction solar cell. The values of J_{sc} and V_{oc} are reasonably good and comparable with those reported in literature. However, the value of FF is lower. Two reasons for the low FF have been identified. First, the series resistance component from the current ITO is high. Note that the quality of the ITO has been optimized for a-Si alloy cells. Since μc-Si:H solar cell has a low V_{oc} and high J_{sc}, it requires higher conductivity ITO to obtain high FF. For the multi-junction solar cell structure in which the current density is relatively low, the role of the ITO resistance is

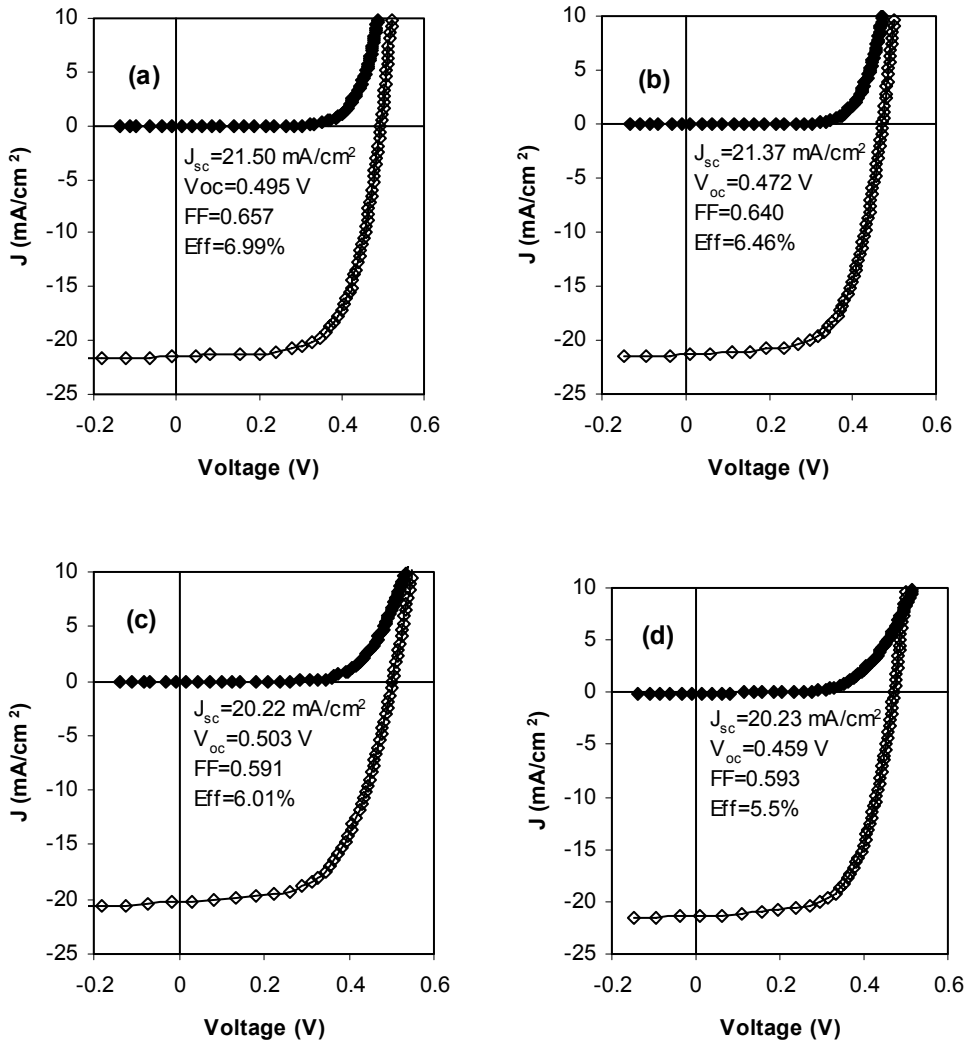

Figure 5. J-V characteristics of μc-Si:H single-junction solar cells deposited using RF glow discharge with different interface layers: (a) with both *n/i* and *i/p* buffer layer, (b), with *n/i* buffer layer only, (c) with *i/p* buffer only and (d) with no *n/i* and *i/p* buffer layers.

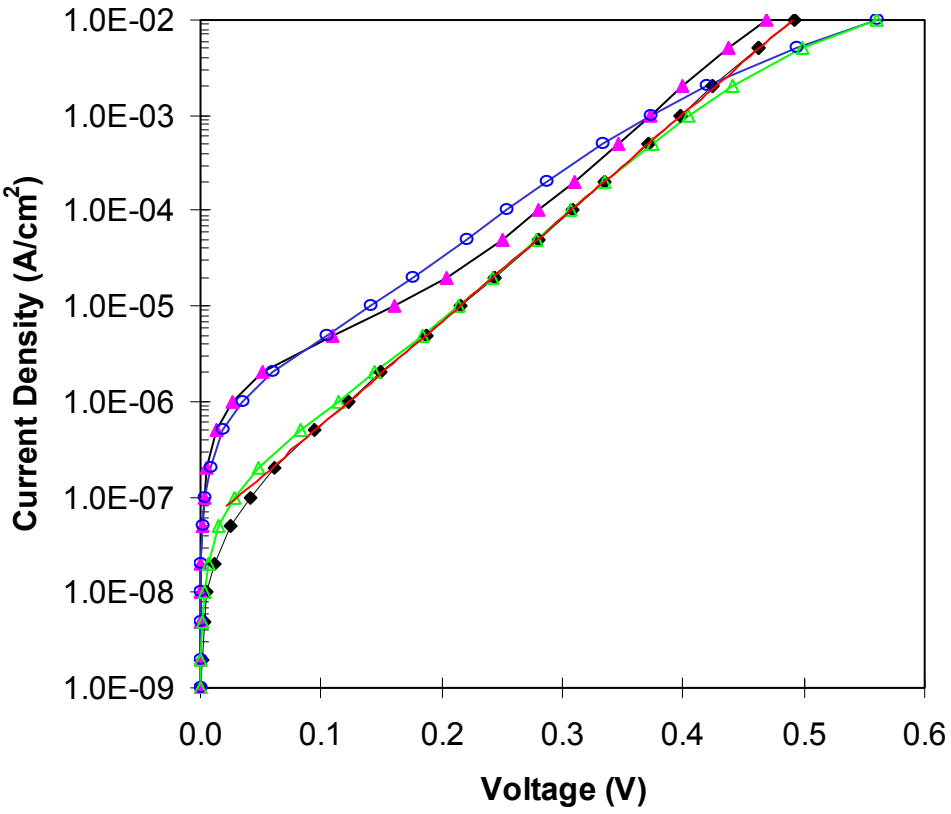

Figure 6. Dark J-V characteristics of μc-Si:H solar cells made with (◆) both *n/i* layer and *i/p* buffer layers, (▲)only *n/i* buffer layer, (△) only *i/p* buffer layer, and (○) no *i/n* and *i/p* buffer layers.

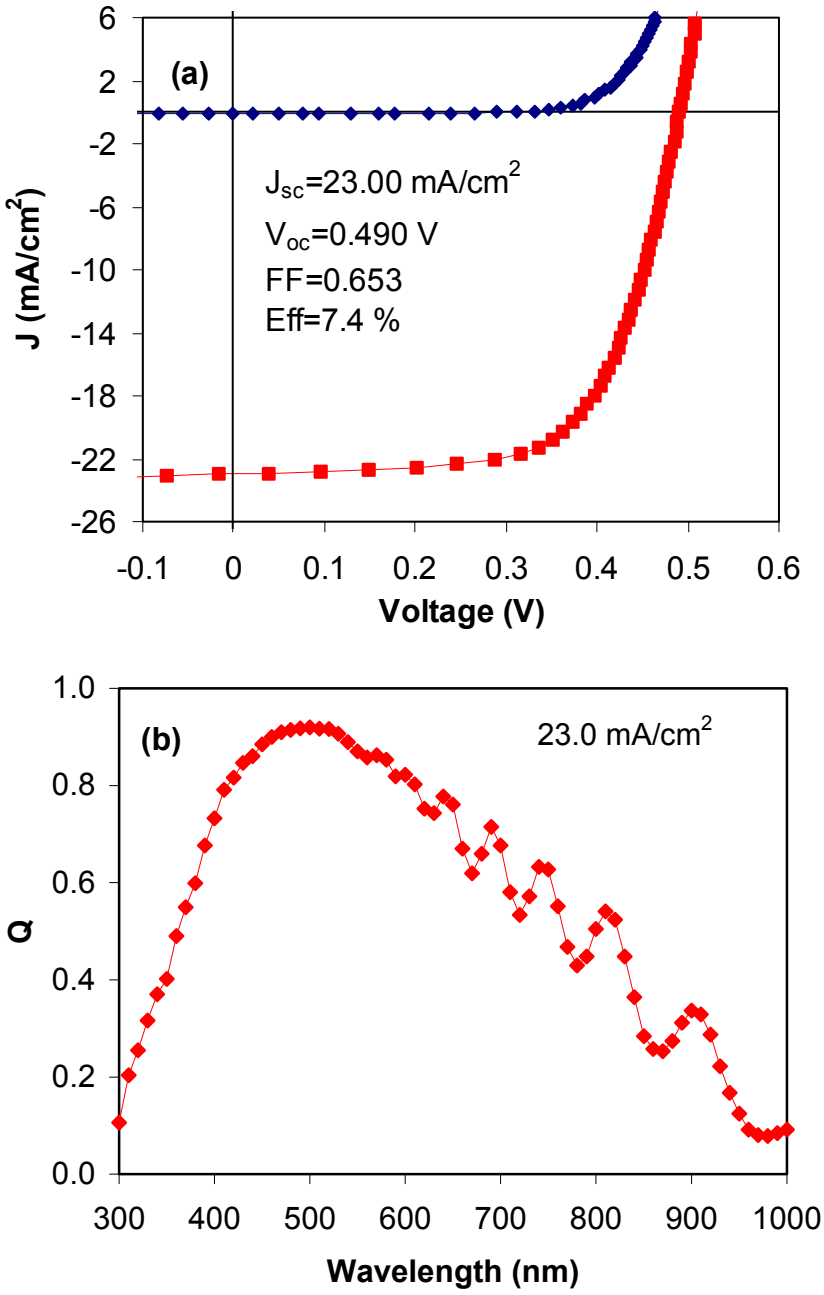

Figure 7. (a) J-V characteristics and (b) quantum efficiency of a μc-Si single-junction solar cell made using RF glow discharge at low deposition rate.

not as critical. Since the ultimate goal is to produce multi-junction cells based on μc-Si:H, we did not change the deposition conditions for ITO. Second, for a single-junction μc-Si:H cell, the quality of the intrinsic μc-Si:H layer may degrade due to atmospheric impurity diffusion after the cell is exposed to the atmosphere post fabrication. Experimental results show that an a-Si:H alloy top cell deposited on top of the μc-Si cell can provide a cap to prevent post-deposition impurity diffusion. Therefore, atmospheric contamination of the μc-Si:H cell is a non-issue for the multi-junction structure. Consequently, we did not spend much time to optimize the single-junction μc-Si solar cell. Instead, we used the a-Si:H/μc-Si:H structure to optimize the bottom cell.

2.7. a-Si:H/μc-Si:H double-junction and a-Si:H/a-SiGe:H/μc-Si:H triple-junction cells

As discussed above, there are two advantages of the a-Si:H/μc-Si:H double-junction structure for optimization of the single-junction μc-Si cell. The a-Si:H top cell can serve as a cap to prevent impurity diffusion and no highly conductive ITO is needed. Figure 8 shows (a) the J-V characteristics and (b) quantum efficiency of the best a-Si:H/μc-Si:H double-junction cell with an initial active-area efficiency of 13.0%. The J_{sc} is taken from the quantum efficiency measurement of the bottom cell, which is measured up to 1000 nm. At this wavelength, the cell has a response ~15% indicating that the current contribution of the bottom cell, and thereby the total Q, would be higher if the measurements could go beyond 1000 nm.

The J-V characteristics of the same double-junction cell were also measured under blue light (<585 nm) and red light (>610 nm). Under blue light, light absorption/current generation is predominantly in the top cell. Since the top and bottom cells are connected in series, the external current is limited by the bottom cell. In this case, the measured FF reflects the bottom cell FF under a reduced light intensity. It was found that the bottom cell FF is 0.811, which is much better than the single-junction μc-Si:H shown in Fig. 7. This result suggests that the μc-Si:H bottom cell quality is indeed superior to that of the a-SiGe:H alloy bottom cell. Under red light, the J-V characteristics reflect the top cell performance. The FF of 0.775 is similar to a single-junction a-Si:H top cell under a low light intensity illumination.

Figure 9 shows the J-V characteristics of the best a-Si:H/a-SiGe:H/μc-Si:H triple-junction solar cell with an initial active-area efficiency of 12.1%. The efficiency is lower than the best a-Si:H/μc-Si:H double-junction cell. First, the total current density is not fully used. In order to achieve a high FF, we need a certain amount of mismatch in the current between the top, middle and bottom cells. Since both the a-Si:H top cell and μc-Si:H bottom cell have better FF than the a-SiGe:H middle cell, we designed the middle cell to have a slightly higher current density than the top and bottom cells to obtain a good FF. A design with top or bottom cell limiting the current would probably lead to a higher stable efficiency. In the present case, the FF of the best triple cell is still lower than the best double-junction cell, partly due to an unoptimized tunnel-junction. Also, the total current density is still lower than we expected. In order to obtain a higher efficiency than the best a-Si:H/a-SiGe/a-SiGe:H triple-junction cell, we need over 27 mA/cm^2. To achieve this high current density, we would need an intrinsic layer thickness of over 3 μm, which would take too long to deposit at the low rate. A higher deposition rate is therefore desirable. We have carried out this study using MVHF at high rates.

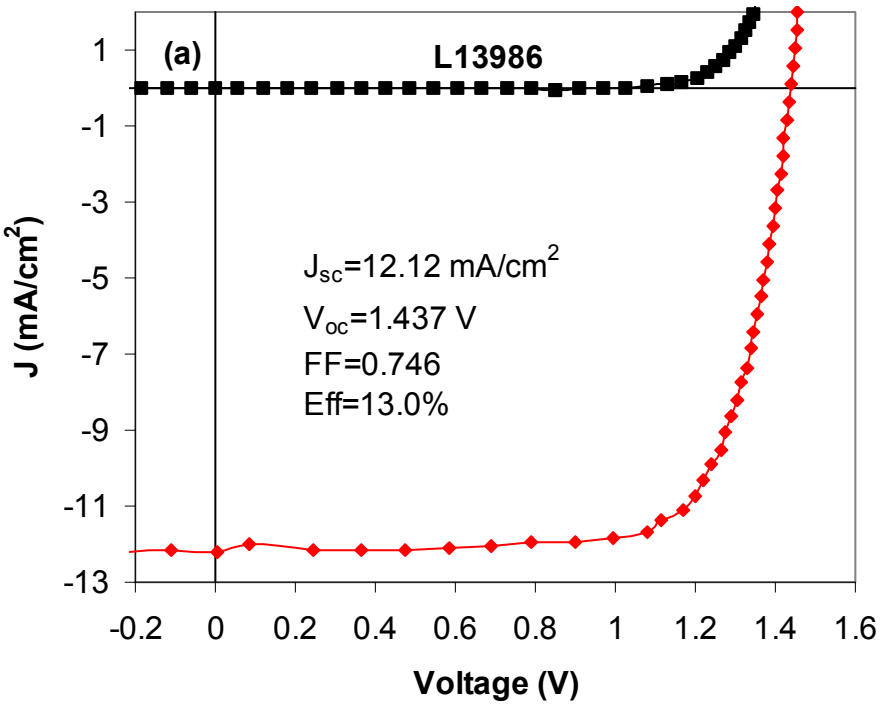

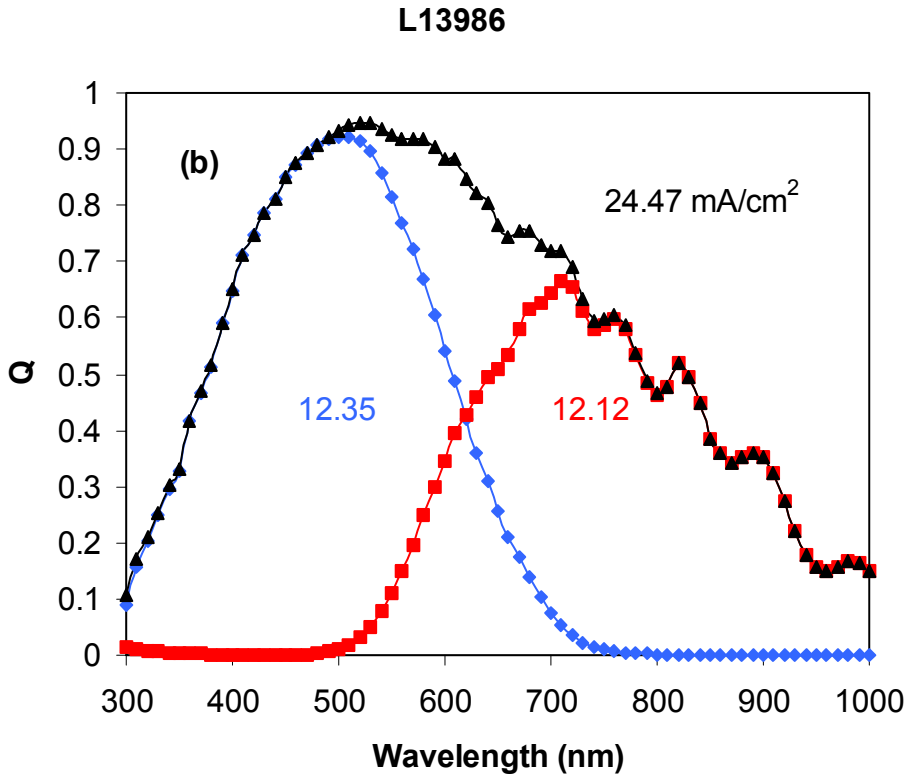

Figure 8. (a) J-V characteristics and (b) quantum efficiency of the best a-Si/μc-Si double-junction cell made using RF glow discharge at low rates.

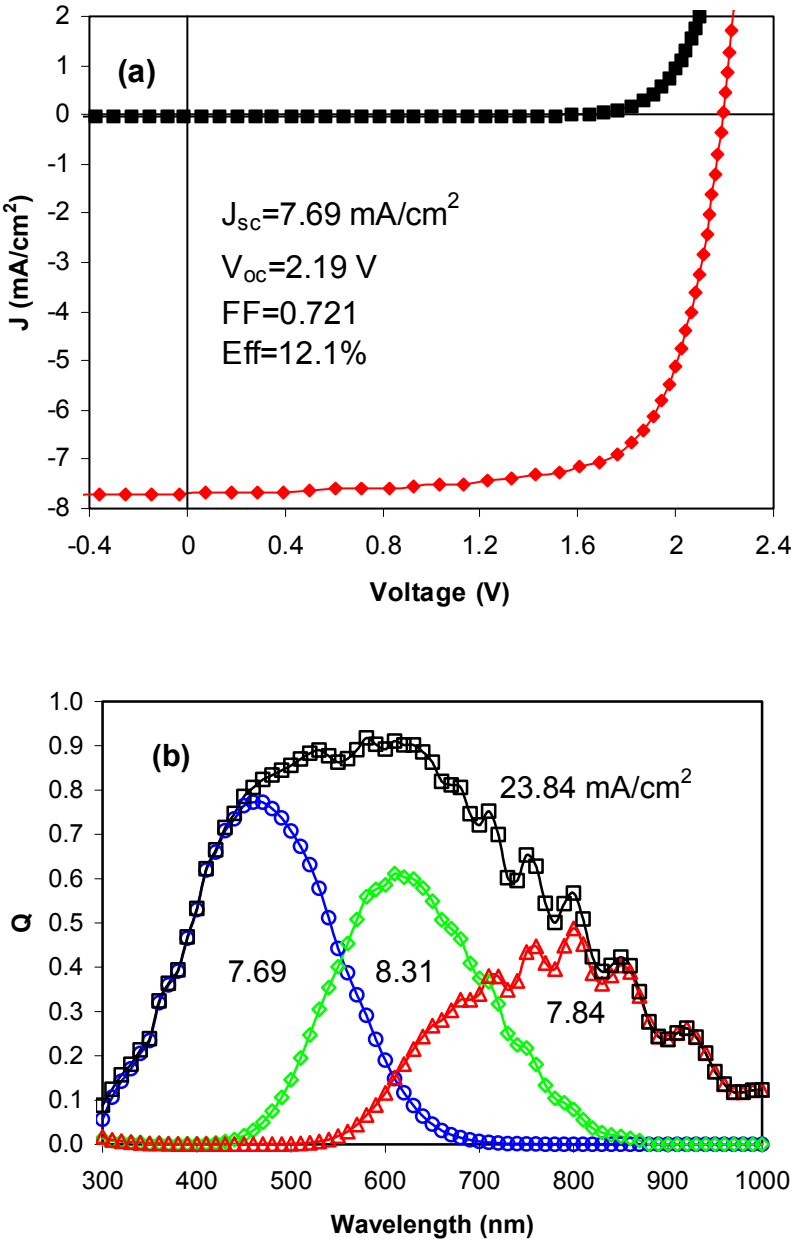

Figure 9. (a) J-V characteristics and (b) quantum efficiency of the best a-Si:H/a-SiGe:H/μc-Si:H triple-junction solar cells made using RF glow discharge at low rates.

2.8. Summary

We have carried out studies on several aspects of μc-Si:H solar cells using RF glow discharges, such as light trapping effect, thickness dependence of cell performance, carrier transport in μc-Si:H solar cells, and control of the interfaces. We have achieved an initial active-area efficiency of 7.4% using μc-Si:H single-junction structure, 13.% using a-Si:H/μc-Si:H double-junction structure, and 12.1% using a-Si:H/a-SiGe:H/μc-Si:H triple-junction structure.

Section 3

Microcrystalline Silicon Cells Deposited Using Modified VHF Glow Discharge at High Rates

As discussed in the previous section, a relatively thick intrinsic layer (> 1 μm) is necessary to obtain a sufficient photocurrent density. From a commercial point of view, high rate deposition technique for μc-Si:H solar cell is essential for increasing throughput and reducing cost. VHF has been widely used to deposited μc-Si:H solar cells at high deposition rates ~ 10 Å/s. We have used a modified VHF (MVHF) technique to deposit a-Si:H and a-SiGe:H alloy solar cells and achieved encouraging results. The μc-Si:H single-junction and multi-junction solar cells were fabricated in the same MVHF reactor.

3.1. μc-Si:H single junction solar cells

μc-Si:H single-junction solar cells were first optimized individually. The growth mechanism and microstructure of μc-Si:H are quite different from that of a-Si:H. By optimizing the deposition condition, we have successfully overcome the post-oxygen diffusion that causes the ambient degradation of μc-Si:H solar cells. Under this optimized condition, we improved the *n/i* and *p/i* interfaces using suitable buffer layers. We achieved an initial active-area efficiency of 7.1 % with a μc-Si:H single-junction cell deposited at a high rate, where the intrinsic layer deposition time was 50 minutes. Figure 10 shows the (a) J-V characteristics and (b) quantum efficiency of the best μc-Si:H solar cell, which shows a comparable performance to the best μc-Si:H single-junction cell made using RF at low rate. This result proves that MVHF is indeed a promising technique for high rate μc-Si:H deposition.

3.2. a-Si:H/μc-Si:H tandem solar cells

High quality μc-Si:H material is a necessary but not sufficient condition to obtain high cell efficiency. Optimization of the cell structure in terms of current matching of the component cells is also important. We optimized the cell structure by adjusting the thicknesses of the top and bottom cells. First, we keep the top cell thickness constant and change the thickness of the bottom cell. Figure 11 shows the performance of the double-junction solar cells with different bottom cell deposition time from 35 min to 50 min with the same deposition rate. The thickness of the top cell was kept the same. The current densities for the top and bottom cells were taken from the quantum efficiency measurement. Since the top and bottom cells are connected in series, the current of the double-junction device is equal to the current of the current-limiting component cell. One can see that with increasing deposition time of the bottom cell, the current from the bottom cell increases monotonically, while the current from the top cell remains almost the same. The double-junction cells transitioned from bottom cell current limited to top cell current limited at the bottom cell deposition time of 40 min. The conversion efficiency of the cells first increased and then decreased with increasing bottom cell deposition time. As shown in Fig. 11 (a), the highest initial efficiency for the double-junction structure is obtained when the currents of the top and bottom cells are equal.

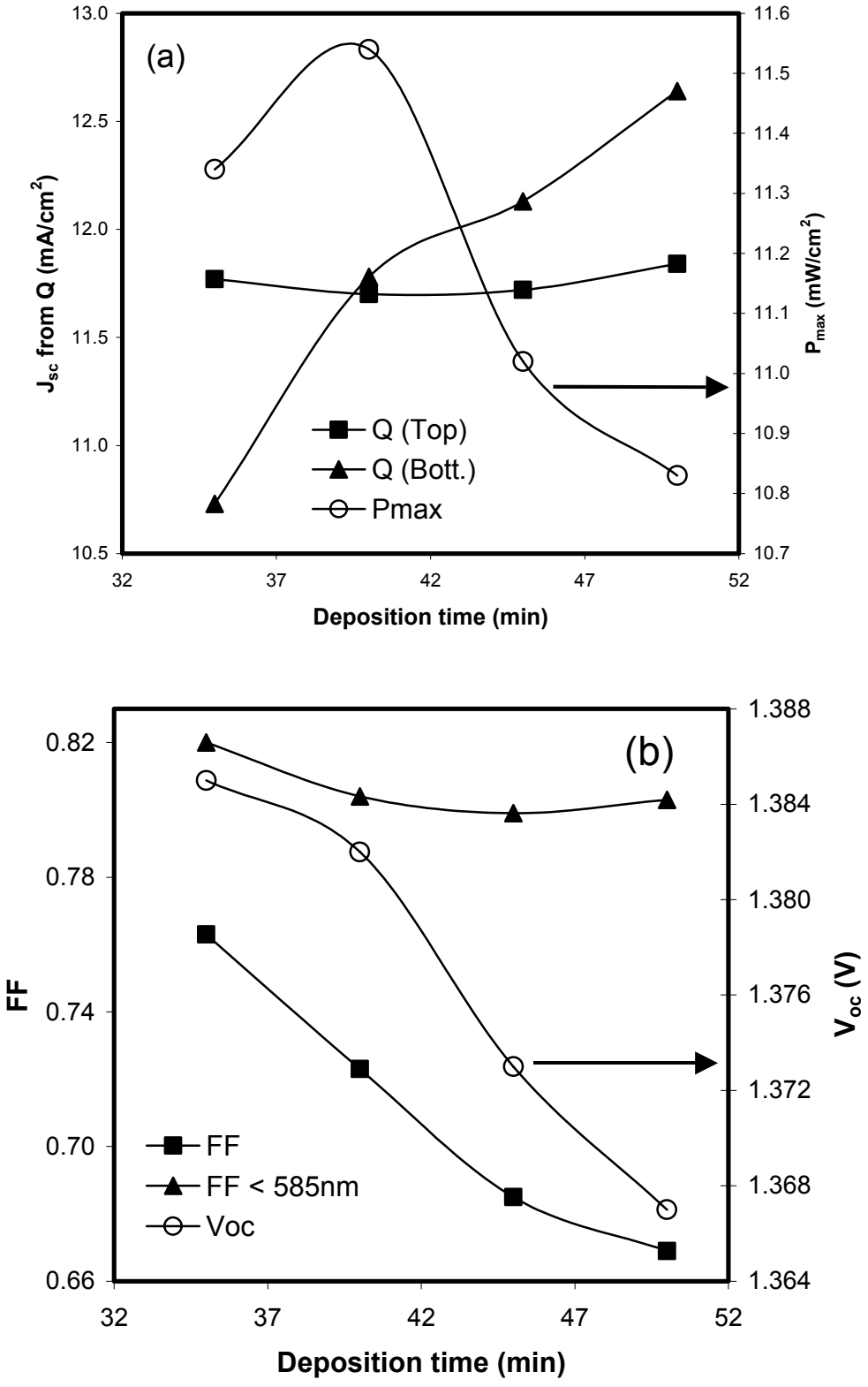

Figure 11. The performances of double-junction a-Si:H/μc-Si:H solar cell vs. μc-Si:H bottom cell deposition time: (a) Q of top and bottom cells and P_{max} and (b) AM1.5 FF, blue FF, and AM1.5 V_{oc}.

Under blue light illumination, photocurrent generation is predominantly in the top cell. The performance of the double-junction cell is governed by the current-limiting bottom cell. Thus, the FF will reflect the quality of the bottom μc-Si:H cell. For the blue light measurement, we used a 585 nm short-pass filter under an AM 1.5 solar simulator. Figure 11 (b) shows that with increasing bottom cell thickness, the blue FF remains somewhat invariant, but the AM1.5 FF decreases from 0.763 to 0.665**.** When the device is strongly bottom cell current limited, the overall FF is limited by the bottom cell and is slightly lower than that measured under blue light due to the weak light intensity under blue filter. When the device is top cell current limited, the overall FF is limited by the top cell. In the strong top cell limited condition, the FF under AM1.5 is 0.665, which is close to the top cell FF when it is deposited on ss. Therefore, in order to obtain a high FF, it is necessary to have a bottom cell limited current mismatch. For this configuration, the overall stability is better too.

In the last section, we presented the results of the relationship between J-V characteristics and the thickness of μc-Si:H layer for single-junction cells. The results showed that an increase in the thickness of the μc-Si:H layer leads to a decrease in the V_{oc}. The V_{oc} behavior of the double-junction cells as a function of the thickness of the μc-Si:H layer (see Fig. 11 (b)) is consistent with the earlier single-junction cell results.

Next, we present the results on another series of samples. This time, we fixed the bottom cell thickness and changed the top a-Si:H cell thickness from a deposition time of 5 min to 8 min. The result is shown in Fig. 12. Increasing the top cell thickness leads to a predictable increase of the top cell current, accompanied by a decrease of the bottom cell current. Both current densities from top and bottom cells tend to level off after 7 min. The current densities of the top and bottom cells are equal for a top cell deposition time of ~ 6 min. Similar to the earlier case (see Fig. 11(a)), the double-junction cell exhibits the highest initial efficiency for the matched current case (see Fig. 12(a)).

Figure 12 (b) shows the FF measured under white and blue light, and V_{oc} measured under white light as a function of the top cell thickness. The results are consistent with the results shown in Fig. 11 (b). The white FF increases with the increase of the top cell thickness since the device changes from top cell limited to bottom cell limited. For the deposition time of 8 min, the double-junction cell is strongly bottom cell current limited. The white FF becomes 0.784, which is mainly due to the high FF from the bottom cell. The V_{oc} of the double-junction cell also decreases with increasing thickness of the top cell and the result is consistent with the case of the single-junction cell.

Based on the above information, we have explored different deposition conditions and designed different cell structures. We have achieved an initial active-area cell efficiency of 12.5%. Figure 13 shows the J-V-characteristics of the a-Si:H/μc-Si:H double-junction solar cells and Fig. 14 plots the J-V characteristics under blue (<585 nm) and red light (>610 nm) illuminations. The blue FF of 0.833 indicates a high quality of the μc-Si:H bottom cell. Once again, the MVHF deposited a-Si:H/μc-Si:H double-junction cell shows a similar performance as the best RF deposited cell at slow rate.

Although high rate deposition for μc-Si:H layer is crucial for solar cell production due to the required intrinsic layer thickness, the proper measure should be the deposition time instead of rate. The argument is that if one can use a relatively thin intrinsic layer without significant loss of current, one may use a lower rate. In addition, a thinner bottom cell results in a bottom

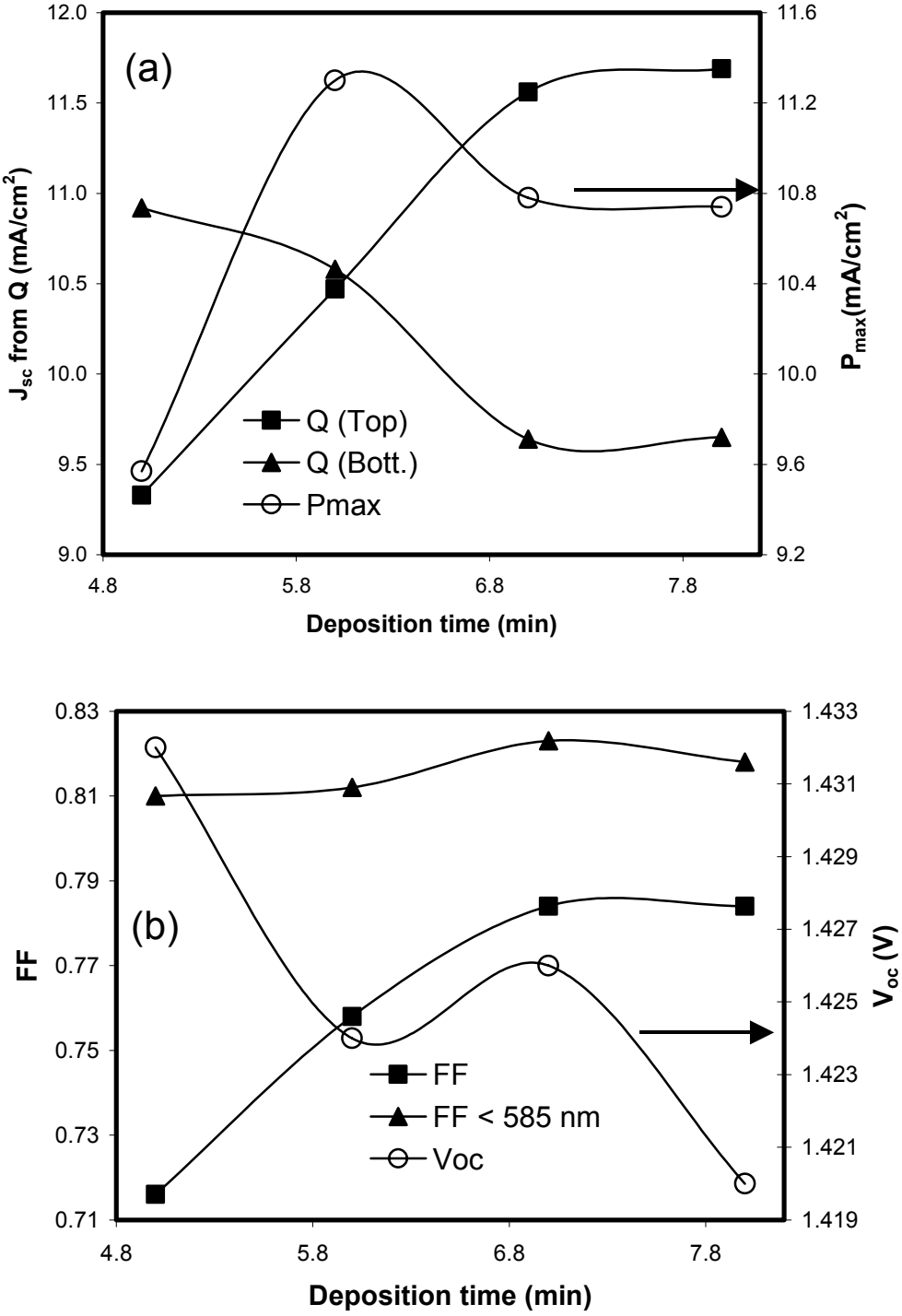

Figure 12. The performances of double-junction a-Si:H/μc-Si:H solar cell vs. μc-Si:H top cell deposition time: (a) Current density from Q of top and bottom cells and $P_{max,}$ and (b) AM1.5 FF, blue FF, and AM1.5 V_{oc}.

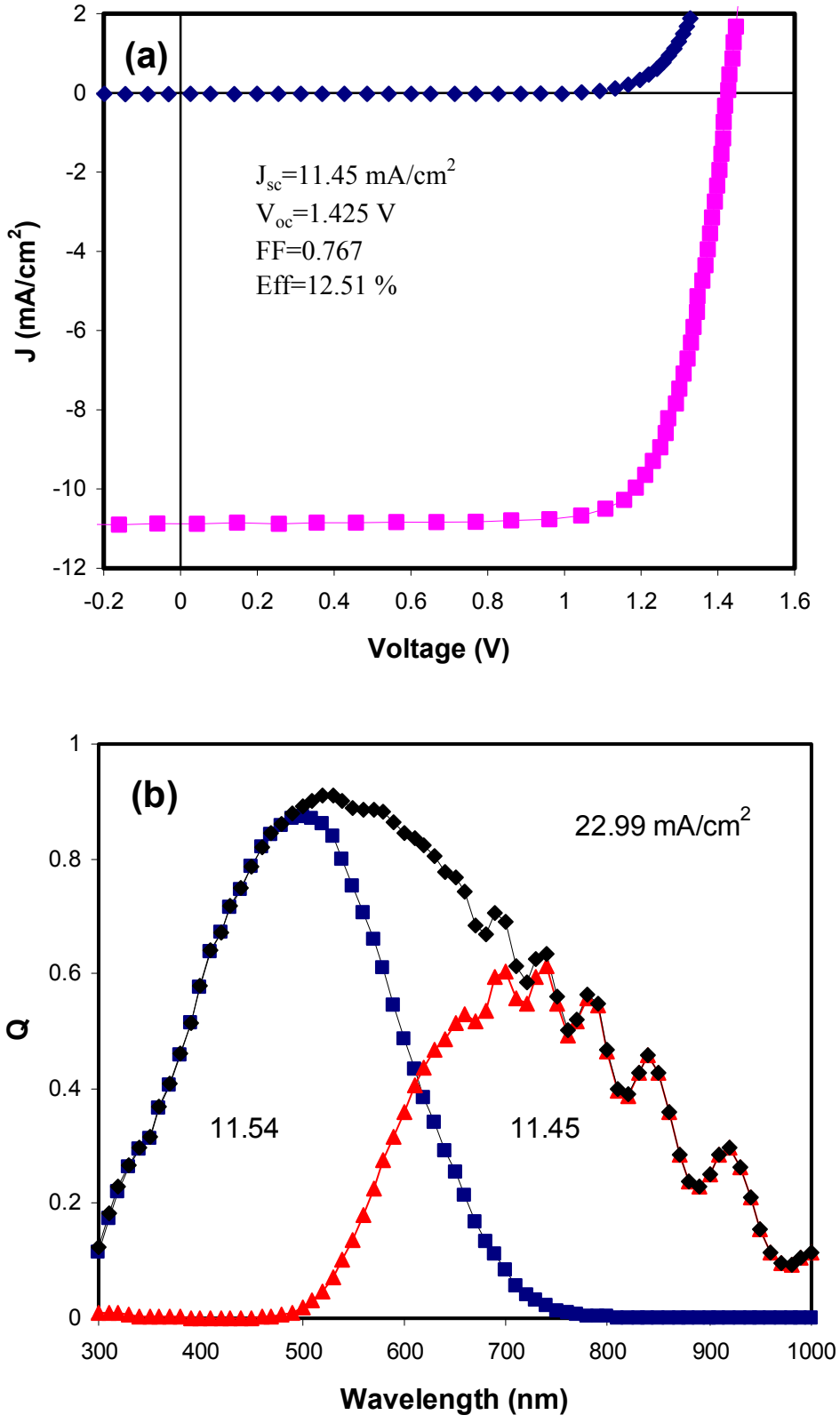

Figure 13. (a) J-V characteristics and (b) quantum efficiency of the best a-Si:H/μc-Si:H double junction cell made with MVHF at a high rate.

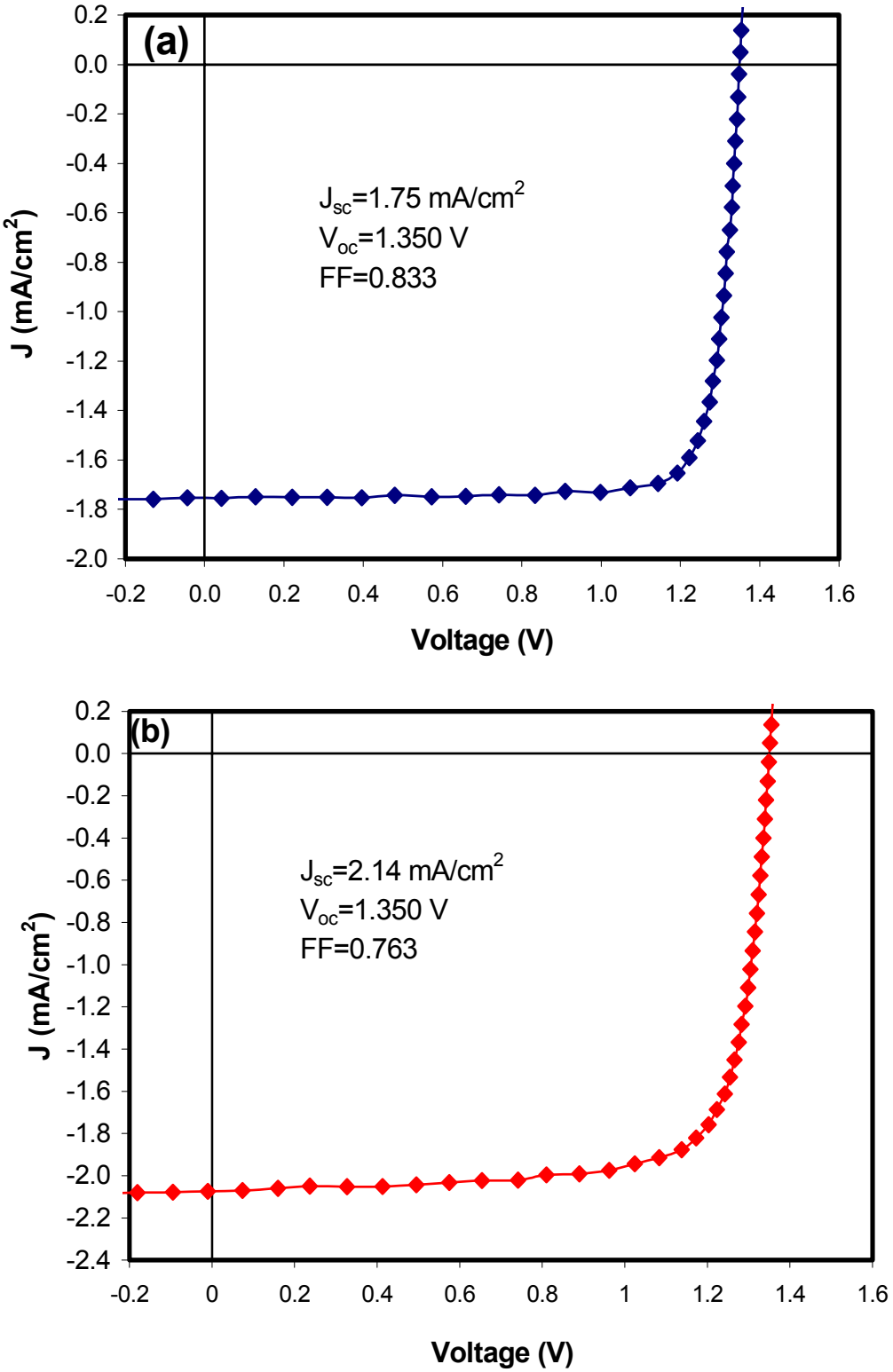

Figure 14. J-V characteristics of the best MVHF deposited a-Si:H/µc-Si:H double-junction cell under AM1.5 illumination with (a) a 585 nm short-pass filter and with (b) a 610 nm long-pass filter.

cell limited current mismatch, hence a better stability. A deposition time ~30min for the μc-Si:H layer is acceptable for the manufacturing environment. Table II lists the J-V characteristics for five solar cells with different bottom cell deposition times. With a bottom cell deposition time of 50 minutes, we achieved an initial active-area efficiency of 12.33 %. By reducing the time to 30 minutes, the efficiency drops to 11.35 %, but the stabilized efficiency is 10.42 % (will be shown in next section).

Table II. J-V characteristics of a-Si:H/μc-Si:H double-junction solar cells made using MVHF with different bottom cell deposition times.

Sample No.	Bottom time (min)	Efficiency (%)	Q(mA/cm^2)		Voc (V)	FF
			Top	Bott.		
12065	210	12.51	11.54	11.45	1.425	0.767
11569	60	12.04	12.09	12.07	1.359	0.734
11635	50	12.33	11.91	11.99	1.392	0.744
11797	35	11.34	11.77	10.73	1.385	0.763
11835	30	11.35	11.19	11.10	1.406	0.727

3.3. a-SiGe:H middle cells

High rate a-SiGe:H middle cells normally are deposited at relatively high substrate temperatures to allow for the impinging radicals to have sufficient mobility on the growing surface, hence reducing microvoid and defect density. However, a high deposition temperature of the a-SiGe:H middle cell during the fabrication of an a-Si:H/a-SiGe:H/μc-Si:H triple-junction structure may have a negative effect on the μc-Si:H bottom cell. In order to prevent degradation of the μc-Si:H bottom cell due to high temperature processing of the subsequent middle cell, the a-SiGe:H layer has to be deposited at the same or lower temperature than the bottom μc-Si:H layer. Therefore, effort was made to optimize the growth conditions of the a-SiGe:H middle cell at low deposition temperatures. a-SiGe:H middle cells were deposited on stainless steel substrate without back reflector. Deposition rate was ~6-8 Å/s. The solar cells were measured under AM1.5 illumination with a 530 nm long-pass filter.

It has been known that the bandgap of the a-SiGe:H alloy depends not only on the Ge/Si ratio, but also on the hydrogen content in the material. Hydrogen content in a-Si:H and a-SiGe:H deposited at low temperature is generally higher than that deposited at high temperature, which leads to the wider a-SiGe:H bandgap and higher V_{oc} in low temperature a-SiGe:H solar cells. In order to maintain a similar V_{oc} (~ 0.75 V), the Ge/Si ratio has to be increased. However, increase of Ge/Si ratio leads to a more defective a-SiGe:H material that in turn results in poor fill factor, FF. All these factors were taken into account in order to attain the optimized growth conditions, such as, plasma power, GeH_4 flow profiling, and GeH_4/SiH_4 ratio. Table III lists the J-V characteristics of three a-SiGe:H solar cells. Sample 11389 was made at a high deposition temperature under an optimized condition. Sample 11798 was deposited under the same condition as sample 11389 except for different substrate temperatures and GeH_4/SiH_4 ratios. The sample 11886 was made under the optimized conditions at low temperature. Compared to the sample 11798, one can see that J_{sc} of the sample 11886 is increased from 7.49 to 7.73 mA/cm^2.

Table III. J-V characteristics of a-SiGe:H middle cells made under different conditions. The measurement were made under AM1.5 illumination with a 530 nm long-pass filter

Sample No.	T	Thickness (nm)	V_{oc} (V)	FF	J_{sc} (mA/cm^2)	P_{max} (mW/cm^2)
11389	High	200	0.754	0.659	8.55	4.22
11798	Low	133	0.751	0.676	7.49	3.71
11886	**Low**	**153**	**0.756**	**0.680**	**7.73**	**3.97**

The FF is slightly higher indicating an improvement of the material quality. However, the J_{sc} of sample 11886 is about 0.8 mA/cm^2 lower than that of the best high temperature cell.

3.4. a-Si:H/a-SiGe:H/μc-Si:H triple-junction solar cell

One factor that limits the solar cell efficiency of the a-Si:H/a-SiGe:H/a-SiGe:H triple-junction structure is the quality of the a-SiGe:H alloy bottom cell. This problem is more serious for high deposition rate cells than for low deposition rate cells. The performance of high-rate a-SiGe:H alloy solar cell decreases more rapidly with the increase of Ge content than low rate a-SiGe:H alloy solar cell. The rapid degradation in the film quality for the high-rate case may be attributed to inadequate time for the GeH_3 radicals to relax on the growing surface. We have explored μc-Si:H solar cell as a possible substitute for the a-SiGe:H cell. Considerable progress has been made in the fabrication of high-efficiency μc-Si:H solar cells. Preliminary work has been done on the optimization of the triple-junction cell structure, a-Si:H/a-SiGe:H/μc-Si:H. The deposition rate for the μc-Si layer is 3-5 Å/s, and the deposition time is 40-60 minutes. The deposition rates for the top and middle cell intrinsic layers are ~ 8 Å/s and ~ 6 Å/s, respectively.

Figure 15 shows the (a) J-V characteristics and (b) quantum efficiency of a high-rate a-Si:H/a-SiGe:H/μc-Si:H triple-junction cell. All the component cells have been prepared by the MVHF technique. The V_{oc} and FF are lower than expected. For this cell, the intrinsic a-SiGe:H layer was deposited at a temperature higher than that for the μc-Si:H film, which may have damaged the bottom cell. In addition, the tunnel junction may also have problem. Further optimization is under way.

3.5. Summary

In summary, we have worked on the optimization of growth conditions and cell structures for μc-Si:H single-junction and a-Si:H/μc-Si:H double-junction solar cells using MVHF method at high growth rates. We have achieved an initial active-area cell efficiency of 7.1 % using μc-Si:H single-junction structure and 12.5% using a-Si:H/c-Si:H double-junction structure. An initial active-area efficiency of 11.3 % has been achieved using a-Si:H/μc-Si:H double-junction structure with a 30-minute deposition time for the μc-Si:H layer. The a-SiGe:H middle cell for incorporation in the triple-junction solar cell has also been optimized at low substrate temperature. Preliminary result on the a-Si:H/a-SiGe:H/μc-Si:H triple-junction solar cell is presented.

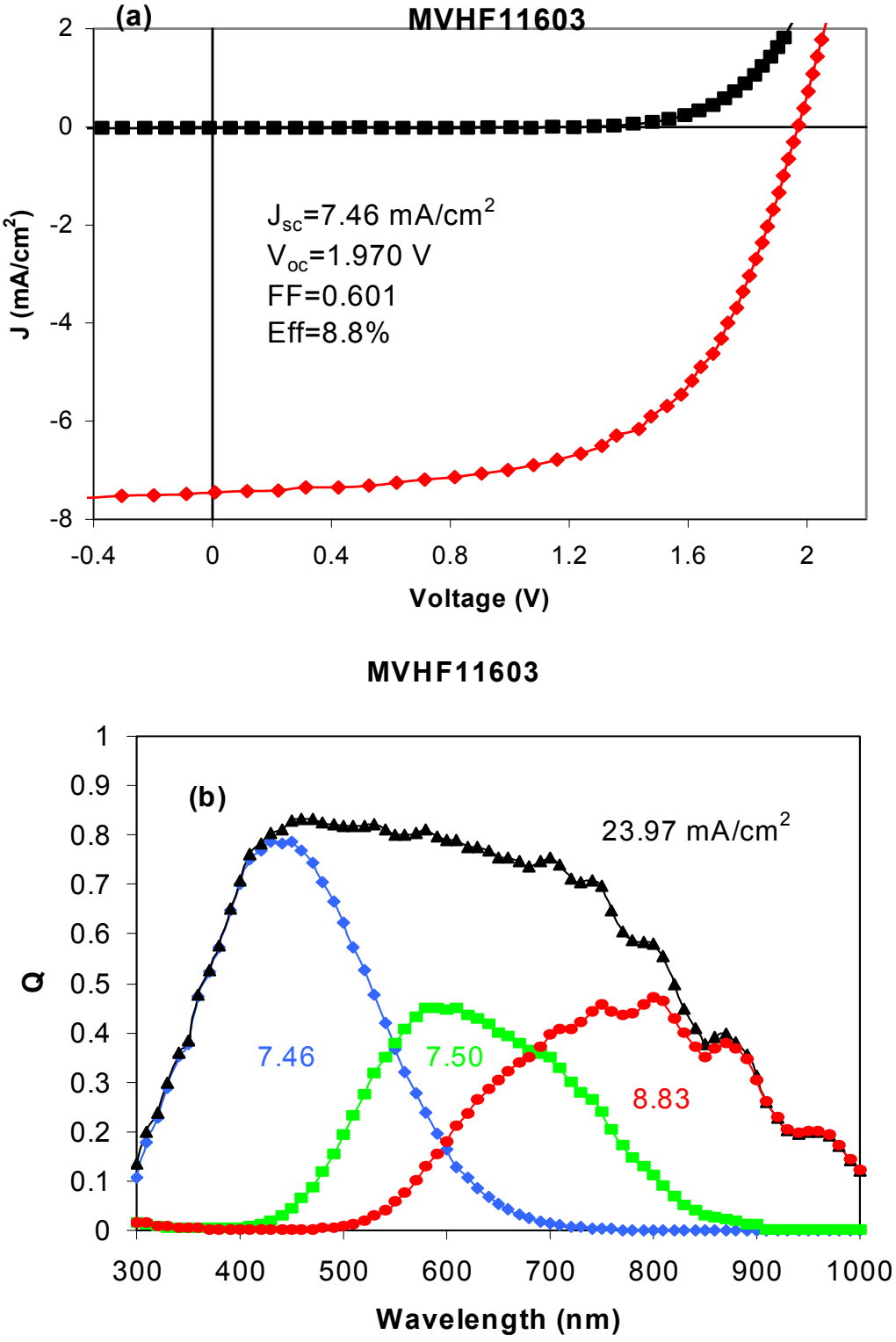

Figure 15. (a) J-V characteristics and (b) quantum efficiency of a MVHF high rate a-Si/a-SiGe/μc-Si triple-junction solar cell.

Section 4

Stability a-Si:H/μc-Si:H Double-Junction Solar Cells

4.1. Introduction

Optimized μc-Si:H solar cells have better stability against light soaking than a-Si:H or a-SiGe:H solar cells. However, in an a-Si:H/μc-Si:H structure, the a-Si:H top cell is usually over 300 nm thick to match the current from the μc-Si:H bottom cell. A thick a-Si:H solar cell usually shows a large degradation after light soaking. With the *i* layer thickness of over 300 nm, the degradation is in the range of 20 - 40% for a single-junction a-Si:H solar cell; the amount of degradation depends on deposition conditions, especially the deposition rate. Therefore, the stability of a-Si:H/μc-Si:H is still questionable, and experimental data are needed to clarify the concern. From our experience on a-Si:H and a-SiGe:H multi-junction cell studies, we know that a top cell current mismatch (a-Si:H top cell usually has better stability than a-SiGe:H middle and bottom cells) can improve the stable efficiency of multi-junction solar cells. In the a-Si:H/μc-Si:H case, the bottom cell has better stability than the top cell, thus a bottom cell limited a-Si:H/μc-Si:H double-junction cell should have a better stability than a top cell limited one.

4.2. Experimental results and discussion

We have carried out light-soaking studies using a-Si:H/μc-Si:H double-junction cells with different current mismatches. a-Si:H/μc-Si:H double-junction solar cells deposited using RF and MVHF with different current mismatches were light soaked under a 100 mW/cm^2 white light at 50 °C for over 1000 hours. The J-V characteristics were measured at different light soaking times. The data is summarized in Table IV. For comparison, an a-Si:H/a-Si:H cell is also included in the table as a reference. The RF low rate cell (13986) has the best initial efficiency of 13.0%, which has a matched current density between the top and bottom cells in the initial state. This cell degraded by 16.2% and reached a stable efficiency of 10.9%. Another RF low rate cell (14066) has a large current mismatch with the bottom cell limiting the current. Even though the initial efficiency is lower than 13986, this cell only degraded by 9.3%, and reached a stable efficiency of 11.2%. The stable efficiency of this cell turns out to be better than the one with the highest initial efficiency. Similar behavior in terms of current mismatch and stability is found for MVHF high rate cells 11570 and 11568. The cells with a large current mismatch (11568) degraded less than the one with matched current (11570). The cells with 40 minutes (11834) and 30 minutes (11835) bottom *i* layer deposition times show the highest stable active-area efficiency of 10.4%. The small degradation of cell 11834 is due to large current mismatch. Figure 16 shows the (a) J-V characteristics and (b) quantum efficiency of cell 11834 at the initial and stable states. From the Q curves, one can see that the bottom cell current did not change after light soaking. Cell 11835 has a thinner a-Si:H top cell. Although the current mismatch is not very large for this cell, the degradation is low possibly due to the superior stability of the thinner top cell.

From this study, we conclude that a bottom-cell limited a-Si:H/μc-Si:H double-junction cell has better stability than a top-cell limited or current matched ones. Figure 17 plots the initial

Table IV. Stability of a-Si:H/μc-Si:H solar cells made using RF at low rates and MVHF at high rates. As a reference, a low rate RF a-Si:H/a-Si:H double-junction cell is also listed. The underlined data indicate the limiting current.

Sample No.	State	Efficiency (%)	J_{sc} (mA/cm^2)		V_{oc} (V)	FF
			Top	Bott.		
RF 13986	Initial	12.99	12.35	<u>12.12</u>	1.437	0.746
	Stable	10.88	<u>11.57</u>	11.88	1.405	0.669
	Degradation	16.2 %	6.3 %	1.9 %	2.2 %	10.3 %
RF 14066	Initial	12.29	12.15	<u>11.31</u>	1.420	0.765
	Stable	**11.15**	11.48	<u>11.25</u>	1.396	0.710
	Degradation	9.3 %	5.5 %	0.5 %	1.7 %	7.2 %
MVHF 11570	Initial	11.76	12.09	<u>12.07</u>	1.359	0.717
	Stable	9.30	<u>11.37</u>	12.11	1.323	0.618
	Degradation	20.9%	6.0%	-0.3%	2.6%	13.8%
MVHF 11568	Initial	11.62	12.15	<u>10.96</u>	1.386	0.765
	Stable	10.24	11.47	<u>10.89</u>	1.351	0.696
	Degradation	11.9%	6.1%	0.6%	2.5%	9.0%
MVHF 11834	Initial	11.30	12.09	<u>10.77</u>	1.404	0.747
	Stable	**10.42**	11.70	<u>10.67</u>	1.374	0.711
	Degradation	7.8%	3.2%	0.9%	2.1%	4.8%
MVHF 11835	Initial	11.35	11.19	11.10	1.406	0.727
	Stable	**10.42**	<u>10.85</u>	10.96	1.378	0.697
	Degradation	8.2%	3.0%	1.3%	2.0%	4.1%
a-Si/a-Si RF 7361	Initial	11.66	<u>8.13</u>	8.15	1.975	0.726
	Stable	**9.70**	<u>7.88</u>	7.99	1.914	0.643
	Degradation	16.8 %	3.1 %	2.0 %	3.1 %	11.4 %

and stable efficiency versus the current mismatch defined as J_{sc}(top) / J_{sc}(bottom) for a-Si:H/μc-Si:H double-junction cells with a similar top cell thickness. It shows that reducing the bottom-cell current causes a lower initial efficiency, but the stable efficiency is not affected significantly. Another advantage of bottom-cell limited structure is that the bottom cell can be made thin in a relatively short time, resulting in a better FF.

A μc-Si:H limited current mismatch also results in a faster stabilization during light soaking. An example of light-soaking kinetics for cells with different current mismatches is shown in Fig. 18, where the bottom-cell limited (MVHF 11570) degraded much less than the current matched one (MVHF 11568). In addition, the bottom-cell limited a-Si:H/μc-Si:H double-junction cell stabilized after about 20 hours, but the current matched one needed about 100 hours to reach stabilized state.

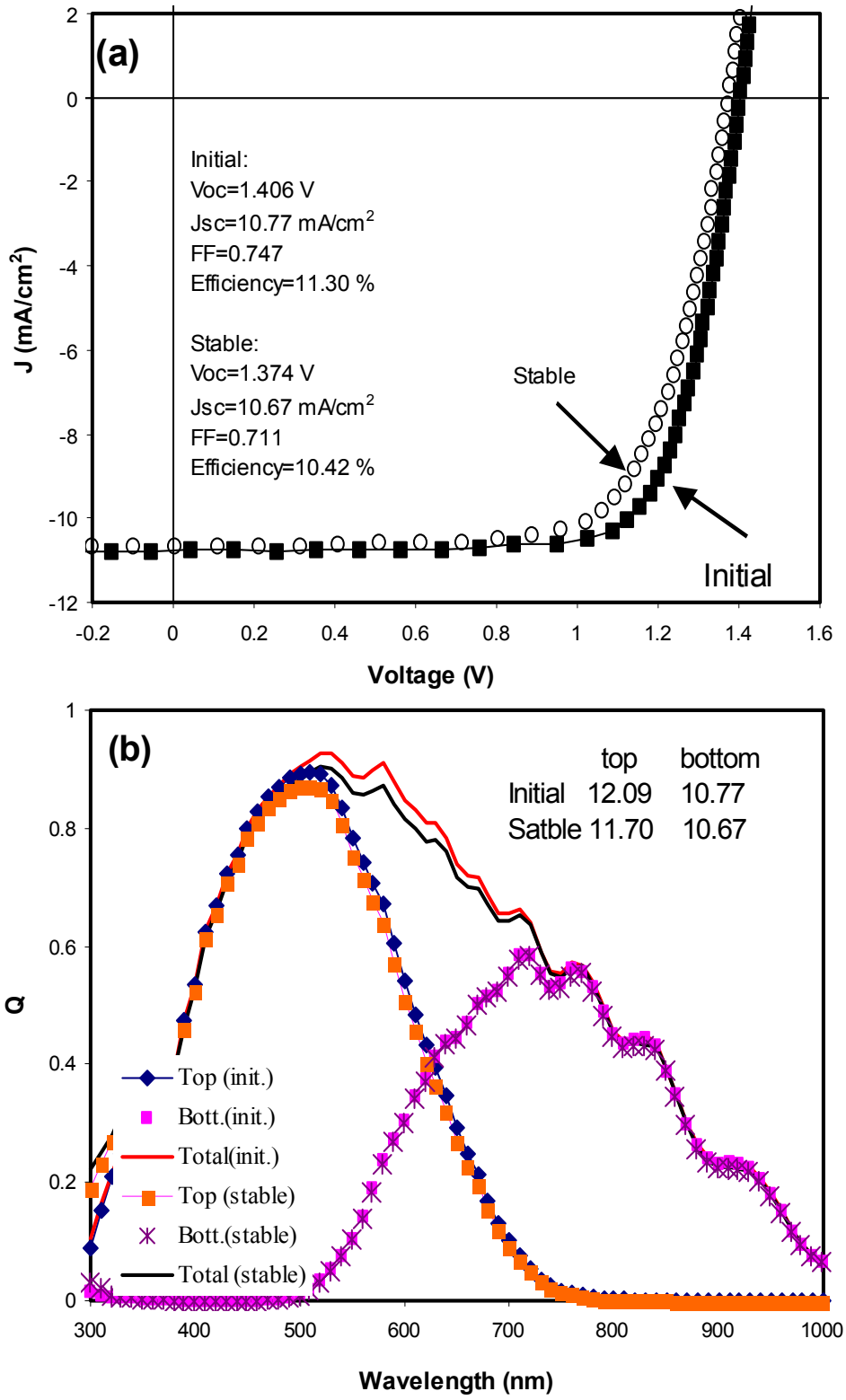

Figure 16. (a) J-V characteristics and (b) quantum efficiency of cell 11834 for the initial and stabilized states.

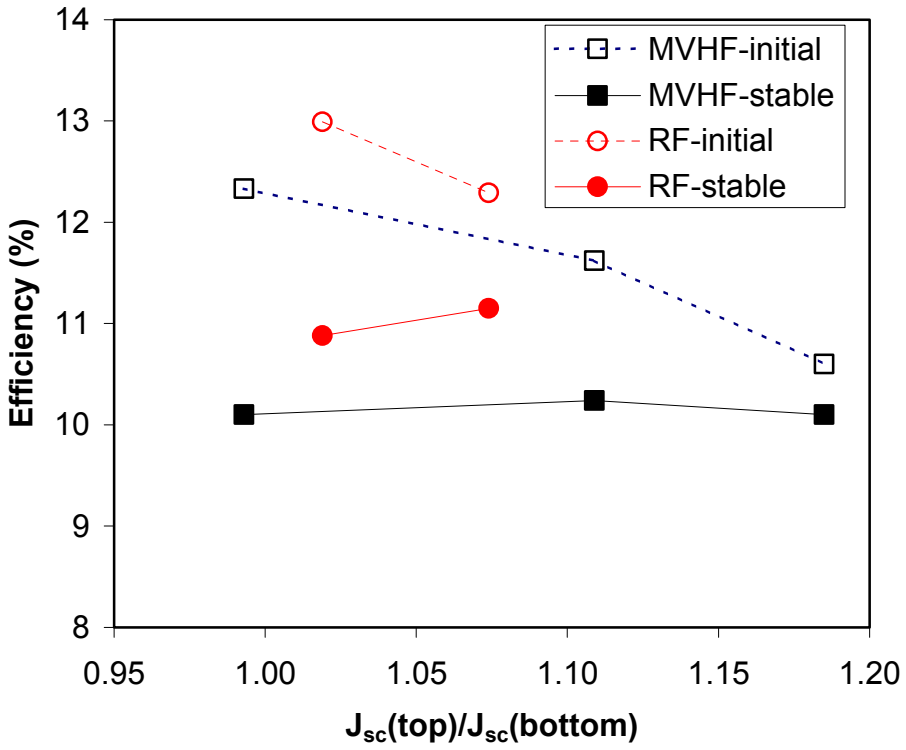

Figure 17. Initial (open symbols) and stable (solid symbols) efficiencies as a function of current mismatch for cells made with RF (circles) and MVHF (squares).

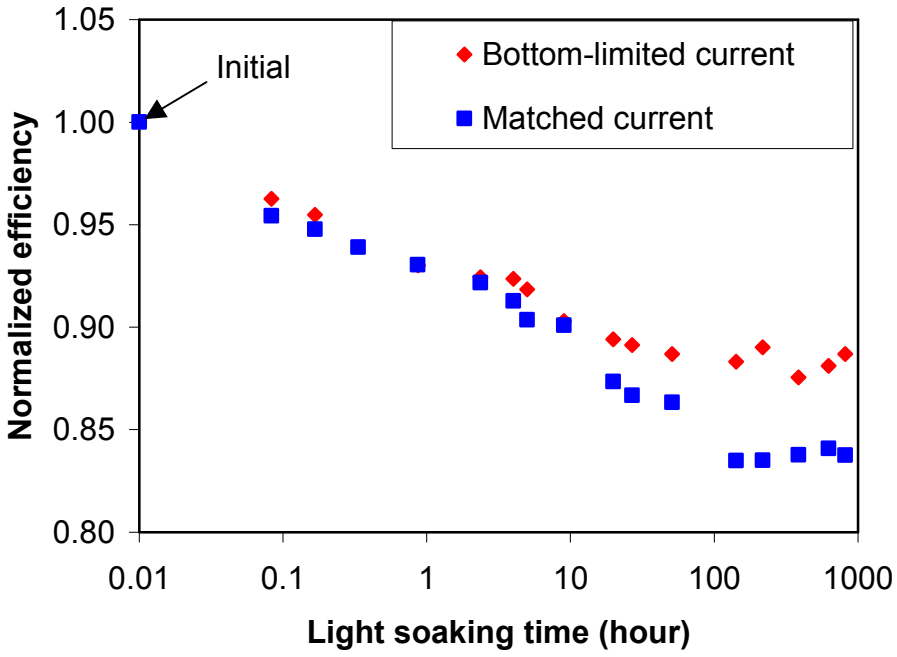

Figure 18. Kinetics of normalized cell efficiency for two a-Si:H/μc-Si:H double-junction solar cells with different current mismatches.

Section 5

Metastability Mixed-Phase Silicon Solar Cells

5.1. Introduction

It has been reported that the best a-Si:H solar cells are deposited with a high hydrogen dilution near the edge of amorphous-to-microcrystalline transition, but on the amorphous side; the best μc-Si:H solar cells, however, are deposited near the edge of microcrystalline-to-amorphous transition, but on the microcrystalline side. The solar cells deposited under conditions between the two edges is defined as mixed-phase cells with characteristics of dramatic changes in V_{oc} upon changes of hydrogen dilution and a large spatial dispersion of V_{oc} over the substrate. Previously, we reported a large increase in V_{oc} after light soaking of mixed-phase solar cells. The amount of the increase depends on the initial V_{oc} and light soaking conditions. A light-induced V_{oc} increase of as large as 150 mV has been observed for a mixed-phase cell. Light soaking under reverse bias and forward current injection experiments suggests that the light-induced V_{oc} increase has the same origin as the Staebler-Wronski effect. We proposed that light-induced crystal volume fraction or grain size reduction could cause the V_{oc} increase. However, recent studies by Raman Spectroscopy and X-Ray Diffraction found no observable change before and after light soaking within experimental errors. Therefore, it is necessary to investigate if the proposed light-induced microcrystalline volume fraction changes is the only reason for the light-induced V_{oc} increase, or other unknown mechanisms exist.

We developed a model to explain the light-induced V_{oc} increase in mixed-phase solar cells. We first analyzed what determines the initial V_{oc} in a mixed-phase solar cell and then proposed the possible causes of the light-induced V_{oc} increase. The new model is consistent with most of the experimental results. In addition, we carried out experiments with different a-Si:H buffer layers for confirmation of the validity of the model. In order to gain more insight into the light-induced V_{oc} increase, we did kinetics measurements of the mixed-phase solar cells as a function of light soaking time.

5.2. Two-diode equivalent circuit for mixed-phase solar cells

Before discussing the mechanism of light-induced V_{oc} increase, we need to understand what determines the initial V_{oc} of a mixed-phase solar cell. We believe that V_{oc} starts to drop only when the fraction of the crystal phase reaches a certain level, resulting in transport paths characteristic of microcrystalline cells. If we neglect lateral transport, a mixed-phase solar cell can be considered as two individual cells connected in parallel. One cell has the characteristics of a-Si:H cell and the other of μc-Si:H cell. Since the V_{oc} of μc-Si:H cells is much lower than that of a-Si:H cells, the μc-Si:H cell will have positive injection current. In the meantime, the a-Si:H cell still has negative photo current under a bias voltage, which lies between the V_{oc} of μc-Si:H cell and the V_{oc} of a-Si:H cell. The open-circuit condition is reached when the positive current of the μc-Si:H cell and the negative current of the a-Si:H cell have the same magnitude. Since the forward current density is usually very high and increases with bias voltage exponentially, one should expect a very sharp V_{oc} drop when the microcrystalline silicon path

appears. The slope of V_{oc} decrease with respect to the increase of crystal volume fraction depends on the quality of the μc-Si:H cell, basically the forward current density.

Based on this information, we can project the dependence of V_{oc} as a function of microcrystal volume fraction if the J-V characteristics of the a-Si:H and μc-Si:H are known. In order to test this hypothesis, we compared the measured J-V characteristics of an a-Si:H solar cell with a good μc-Si:H cell and a poor μc-Si:H cell, as shown in Fig. 19 (upper curve). Considering a mixed-phase cell with unit area, we multiplied the positive current density data of the μc-Si:H cell with an assumed percentage of crystal volume fraction and multiplied the current density of the a-Si:H cell with the remaining percentage, and obtained the voltage that corresponds to the same current for the μc-Si:H and a-Si:H cells. This voltage is the V_{oc} of the mixed-phase solar cell with the given percentage of microcrystalline phase. For voltages that are larger than a certain value, current density data are not available for the μc-Si:H cell due to the limitation of measurement. In this case, we need to use extrapolated data. To obtain this data, we used an exponential extension and a linear extension. Figure 19 (lower curve) shows the estimated results using the good μc-Si:H cell with both exponential and linear extensions, and using the poor μc-Si:H cell with a linear extension. From this plot, one can see that the V_{oc} drops sharply with increase of crystal volume fraction. The higher the quality of the microcrystalline cell (the fast increase of the current density with voltage), the steeper the decrease of V_{oc}. Based on this plot, we can explain the increase in V_{oc} as follows. First, the crystal volume fraction might be reduced by light soaking, the same as we proposed before. In this case, the movement will be along the curve on the plot (see Fig. 19). Second, the quality of the microcrystalline phase is degraded by light soaking, such as an increase of grain boundary recombination. In this case, the forward injection current is not sufficient to compensate for the photocurrent from the amorphous phase under the initial V_{oc}. Therefore, a larger voltage is needed to reach a new open-circuit condition. In the latter case, the movement is along a line perpendicular to the X-axis (see the upward arrow in Fig. 19 (lower)). This process is consistent with the degradation of FF. In mixed-phase solar cells, the two possible processes may coexist at the same time. Although good μc-Si:H solar cells have been reported to exhibit no light-induced degradation, the mixed-phase μc-Si:H cells do degrade. We believe that our new model satisfactorily explains the observed light-induced phenomenon.

5.3. Buffer layers in mixed-phase solar cells and their effect on metstability

To test the two-diode equivalent circuit model, a new experiment was conducted. a-Si:H buffer layers of various thicknesses were deposited using RF glow discharge between the *p* and *i* layers of a mixed-phase *nip* silicon solar cell. The samples were deposited on Al/ZnO back reflector. Indium tin oxide (ITO) dots of area 0.05 cm^2 and 0.25 cm^2 were deposited on top of the *p* layer as the top contact. Each substrate contains 40 ITO dots on a 4 cm × 4 cm area. The J-V characteristics of the solar cells were measured at their initial and light-soaked states. Light soaking was done under AM1.5 illumination of intensity 100 mW/cm^2 at 25 ºC for 40 hours. Although the cells on one substrate exhibit a large V_{oc} range corresponding to μc-Si:H, mixed-phase, and a-Si:H due to a non-uniform deposition as shown previously, the reproducibility is quite good, i.e. the cells using the same recipe from different runs but at the same location on the substrate have similar characteristics. Therefore, the difference between cells at the same location but with different buffer layer thicknesses is due to the buffer layers. Table V lists the

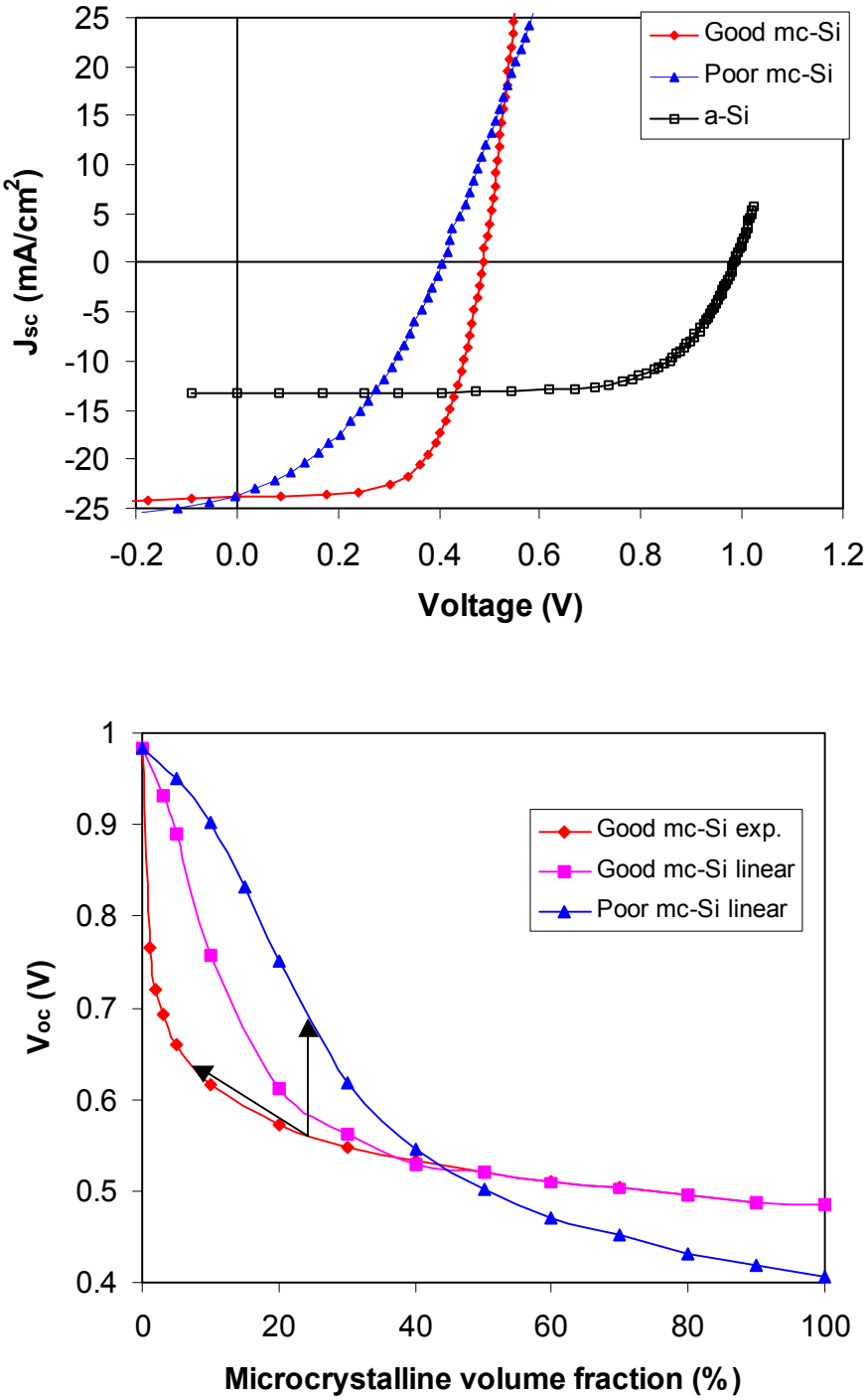

Figure 19. (upper) light J-V characteristics of an a-Si:H and two μc-Si:H cells and (lower) estimated V_{oc} as a function of crystal volume fraction in mixed phase solar cells.

.

initial and light soaked values of the I-V characteristics of three cells with different buffer layer thicknesses but at the same location on the substrate. One can see that the V_{oc} increases from 0.638 V to 0.955 V when the buffer layer thickness is increased from 0-500 Å. It clearly shows the role the buffer layer plays in determining the V_{oc} of the mixed-phase cells. The initial V_{oc} and FF increases even when only a 100 Å buffer layer is deposited, probably due to the reduction of back diffusion, interface recombination, and reduction of shunt current.

In order to understand the effect of the buffer layer on cell performance, dark J-V characteristics were measured at room temperature. Figure 20 shows the dark J-V curves for the three cells listed in Table V. A significant shunt current is observed in the cell with no buffer layer. For the cells with 100 Å and 500 Å thick buffer layers, the buffer layer completely blocked the shunt current, as evidenced by the straight line at $V < 0.5$ V. Therefore, we believe that the increase in initial V_{oc} from no buffer layer to 100 Å thick buffer layer is mainly due to reduced shunt current. In addition, the two cells have the same current for $V > 0.5$ V. This result is consistent with the behavior predicted by the two-diode model based on light-soaking results. The cell with 500 Å buffer layer has a much lower current at $V > 0.5$ V, which means the 500 Å thick buffer layer significantly reduces the forward injection current in the equivalent μc-Si:H diode. As a result, the 500 Å thick buffer layer increases the initial V_{oc} further, but decreases FF significantly due to a thick barrier for hole collection.

As discussed in the previous section, the light-induced V_{oc} increase could be due to the microcrystal volume fraction reduction and forward injection current reduction. Figure 21 compares the dark J-V curves of the cell with 100 Å thick buffer layer at the annealed and degraded states, where the symbols are experimental data and the lines are the fittings for diode characteristic formula. It appears that light soaking increases the current at low voltage (< 0.5 V) due to an increased reverse saturated current and increases the diode quality factor from 1.67 to 2.24. But at high voltage, light soaking decreases the current, a factor partially responsible for the light-induced V_{oc} increase. Figure 22 shows the light-induced changes in V_{oc} for the cells with the three different buffer layer thicknesses as a function of initial V_{oc}. The mixed-phase cells with no buffer layer and with a 100 Å-thick a-Si:H buffer layer have a bell-shaped curve as previously reported. However, no light-induced V_{oc} increase is observed for the cells with a 500 Å thick a-Si:H layer. Instead, V_{oc} decreases after light soaking, similar to regular a-Si:H cells.

Table V. Initial and light-soaked J-V characteristics of three mixed-phase silicon solar cells with different a-Si:H buffer layers.

Buffer layer thickness (Å)	State	J_{sc} (mA/cm^2)	V_{oc} (V)	FF
0	initial	16.7	0.638	0.518
	degraded	15.2	0.684	0.427
100	initial	16.2	0.722	0.584
	degraded	14.7	0.830	0.479
500	initial	16.0	0.955	0.473
	degraded	15.0	0.924	0.426

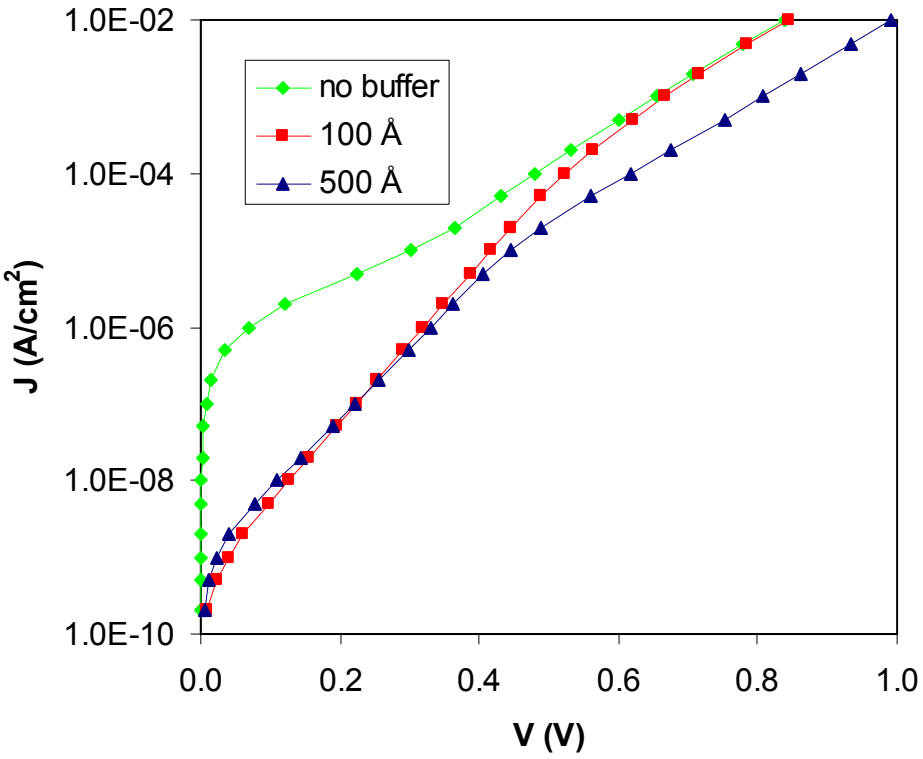

Figure 20. Dark J-V characteristics of the mixed-phase solar cells with different thickness buffer layers.

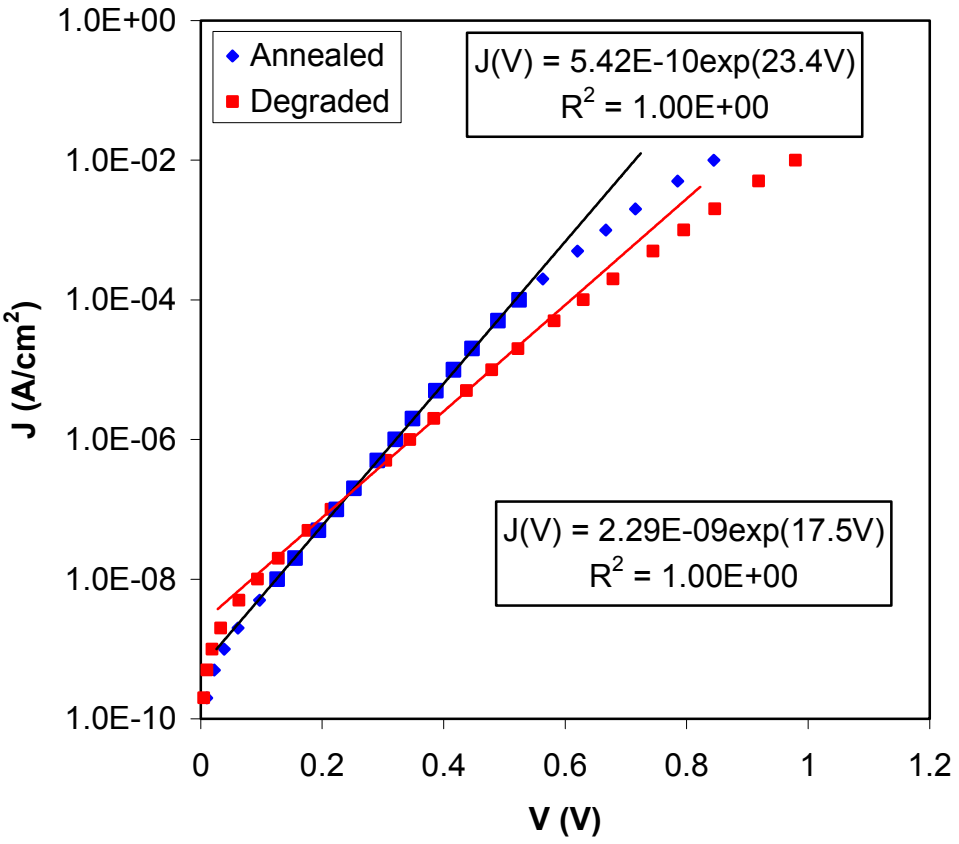

Figure 21. Dark J-V characteristics of a mixed-phase solar cells with 100 nm a-Si:H *i/p* buffer layer at the annealed and degraded states.

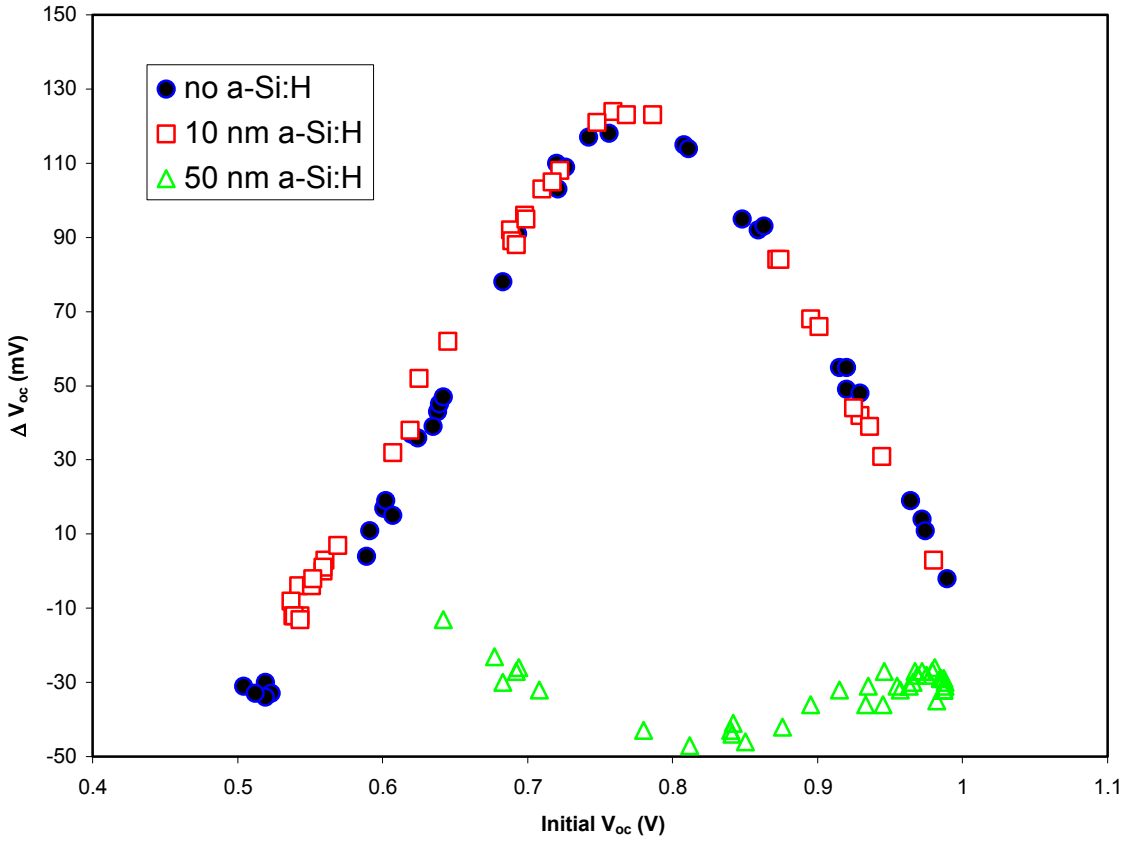

Figure 22. Light-induced V_{oc} change versus initial V_{oc} for cells with different a-Si:H buffer layer thicknesses.

A thick buffer layer between the *p* and *i* layers would reduce the forward current density of μc-Si:H cell significantly by blocking hole injection because of the wider bandgap of a-Si:H compared to μc-Si:H and a large valence band edge discontinuity between a-Si:H and μc-Si:H layers. As discussed above, a low forward current density in the μc-Si:H cell results in a large V_{oc} in a mixed-phase solar cell as shown in Table V. In addition, the forward current density in a μc-Si:H cell with a thick buffer layer is no longer determined by the quality of the intrinsic layer, but instead by the a-Si:H buffer layer. In this case, light-induced changes in the microcrystal quality do not lead to an increase in V_{oc} of the mixed-phase silicon solar cell. The similar characteristics of cells with 0 Å and 100 Å-thick a-Si:H buffer layers indicate that carriers can tunnel through the thin buffer. Similar experiments with a-Si:H buffer layers inserted between the *n* and *i* layers did not show observable effect on the initial V_{oc} or light-induced behavior. The reason could be that V_{oc} is determined by the dominant junction, namely *i/p* junction, in a-Si:H solar cells. Slight change at the *n/i* interface does not significantly affect V_{oc}.

5.4. Kinetics of light-induced V_{oc} increase in mixed-phase solar cells

The light-induced V_{oc} increase depends on cell deposition and measurement conditions. In principle, the metastable behavior is a transition process between two thermal equilibrium states, one is in the dark (or under ambient condition) and the other is under illumination. The kinetics of the metastable changes provides information not only in the two equilibrium states, but also during the transition process. In order to gain the insight into the mechanism of the light-induced V_{oc} increase, we conducted kinetic measurements. Current-voltage (J-V) characteristics as a function of light soaking time were measured at 25 ^{o}C under an AM1.5 solar simulator for cells with various initial V_{oc}. To ensure that the measurement for each cell starts from the initial state, a stainless steel plate with a hole was used to cover all other cells while the exposed cell was being measured. The parameters V_{oc}, FF and J_{sc} were extracted from J-V curves to plot the kinetics curves. All the measurements were computer-controlled.

We first conducted measurements on cells having initial V_{oc} >0.8 V (a-Si:H side). The light-soaking time is about 16 hours (overnight). Figure 23 shows (a) the V_{oc} and (c) FF of the cells with different initial V_{oc} as a function of time. Normalized values of V_{oc} and FF with respect to their initial values are plotted in Figure 23 (b) and (d), respectively. One can see that the V_{oc} ramps up for the cells with V_{oc} < 0.98 V during light-soaking and then saturates. The ramping rate, saturation time and the amount of increase depend on the initial V_{oc}. For the cell with an initial V_{oc} of 0.86 V, the V_{oc} increases by 100 mV after 16 hours of light soaking, and does not saturate. With increasing initial V_{oc}, the rate and the magnitude of increase get smaller and the saturation time becomes shorter. In the mixed-phase solar cells, two competing processes exist in the V_{oc} kinetics during light soaking, i.e. decreasing V_{oc} by Staebler-Wronski effect and increasing V_{oc} due to the reduction of microcrystalline volume fraction and the reduction of forward current in the microcrystalline region. When these two competing processes are balanced, the V_{oc} should not change. The cell with an initial V_{oc} of 0.98 V has this kind of balanced structure. As indicated in the figure, the V_{oc} is almost flat for the first 3 hours, and then decreases slightly. The V_{oc} of the cell with an initial V_{oc} of 1.011 V continuously decreases during light-soaking, a behavior characteristic of conventional a-Si:H solar cells. As shown in Fig. 23 (c), the values of FF for all the cells decrease with time and do not exhibit saturation.

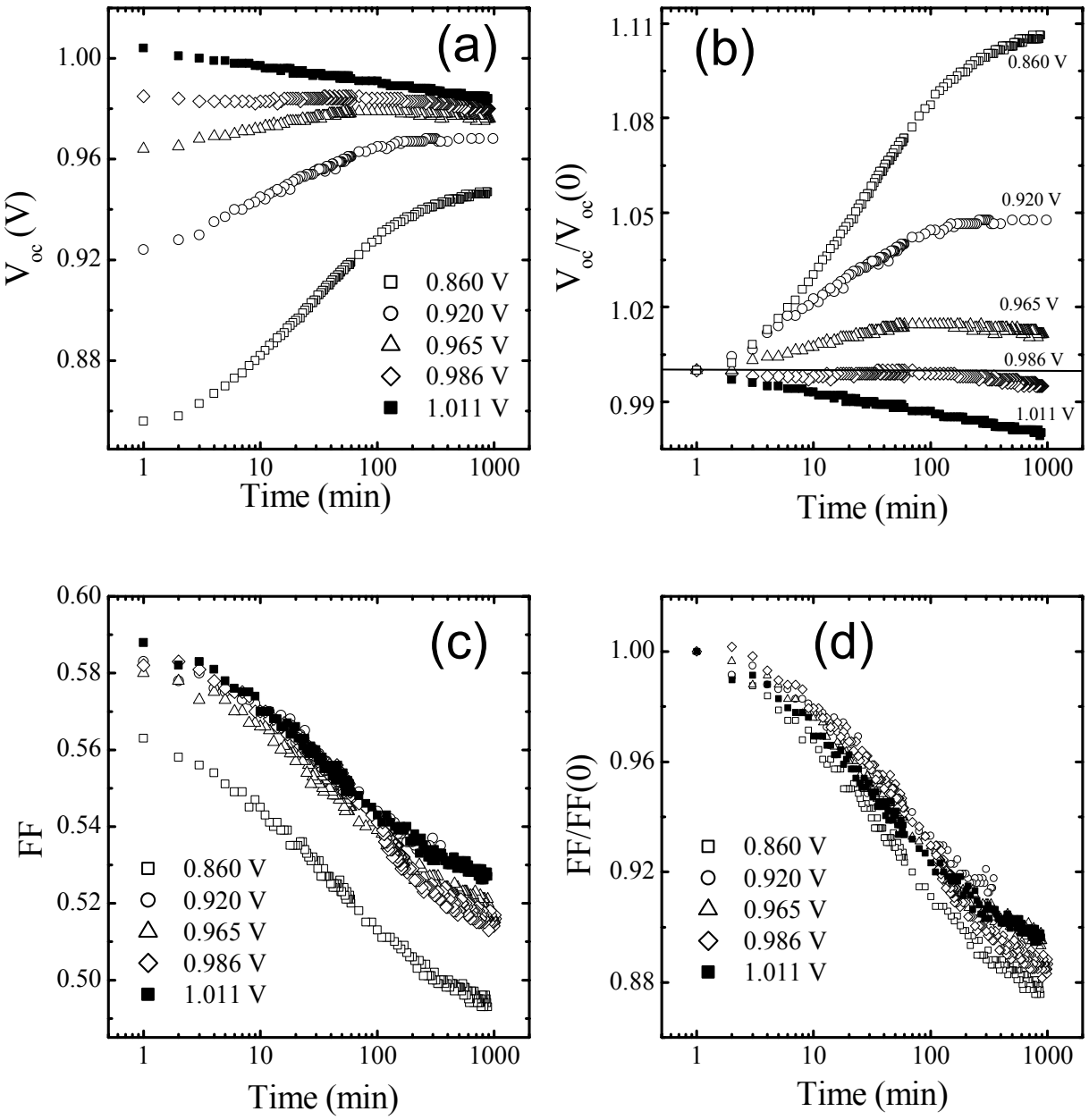

Figure 23. Kinetics of V_{oc} and FF for the cells with various initial V_{oc} on the a-Si side: (a) V_{oc}, (b) normalized V_{oc}, (c) FF, and (d) normalized FF.

The results of the cells having initial V_{oc} less than 0.8 V (μc-Si:H side) are shown in Fig. 24. The V_{oc} increases with time for cells having an initial $V_{oc} > 0.6$ V, but decreases with time for the cells with an initial $V_{oc} < 0.6$ V. In contrast to the behavior of cells on the a-Si:H side, the rate and the magnitude of the change increase with the increase of V_{oc}. Figure 24 (c) shows the changes in FF with light-soaking time. Again, FF decreases with light-soaking time for all the cells. Also, neither V_{oc} nor FF shows saturation.

It is interesting to compare the details about the behavior of the changes of V_{oc} and FF of the two sides. First, we found that the V_{oc} enhancement does not exhibit saturation for cells on the μc-Si:H side but does saturate for cells on the a-Si:H side. Similarly, FF shows a tendency to saturate. Second, compared to the a-Si:H side, the ramping rate of V_{oc} is small at the beginning of light soaking for cells on the μc-Si:H side. For some cells, the V_{oc} does not change after tens of minutes. After passing an intersection point that depends on the initial V_{oc}, the ramp rate of V_{oc} of cells on the μc-Si:H side is faster than on the a-Si:H side.

In order to confirm the above observations, light soaking for a longer time was done on two solar cells. One was selected from the a-Si:H side and the other from the μc-Si side. Figure 25 shows the V_{oc} and FF changes of the two cells with an initial V_{oc} of 0.952 V and 0.590 V over a period of 67 hours of light soak. For the cell with an initial V_{oc} of 0.952 V, the V_{oc} first increases, then appears to saturate, and finally starts to decrease. For the cell with an initial V_{oc} of 0.590 V, the V_{oc} keeps increasing and has no indication of saturation. The FFs of the two cells decrease monotonically with time, but the change for the cell with an initial V_{oc} of 0.952 V is much slower than that with 0.590 V.

In summary, we find that for the cells with initial $V_{oc} > 0.8$ V, the rate of increase of V_{oc} is higher at the beginning of light soaking than that for the cells with $V_{oc} < 0.8$ V. For longer exposure times, the rate of increase of V_{oc} is lower for cells with initial $V_{oc} > 0.8$ V than that for cells with $V_{oc} < 0.8$ V. The two sets of curves intersect at a certain exposure time that is determined by the value of the initial V_{oc}. The cells with initial V_{oc} larger than 0.8 V exhibit saturation after long time of light soaking. For some cells with initial V_{oc} in the range 0.95-0.98 V, the V_{oc} shows an initial increase followed by a decrease. For cells with $V_{oc} < 0.8$ V, the V_{oc} does not exhibit saturation for exposure time up to 1000 min. All cells show decreases in FF with exposure time. The cells with $V_{oc} > 0.8$ V show earlier saturation than those with $V_{oc} < 0.8$ V.

A similar behavior is observed in the dependence of change in V_{oc} (ΔV_{oc}) on initial V_{oc} for different light-soaking times. As shown in Fig. 26, ΔV_{oc} increases with light-soaking time for all cells. Also, the position of the peak shifts towards lower initial V_{oc}. The cell with an initial V_{oc} of 0.86 V exhibits the highest change after exposure time of 5 minutes. The cell with an initial V_{oc} of 0.77 V exhibits the highest change after exposure time of 40 hrs. This phenomenon is indicative of a faster initial V_{oc} increase in the cells with higher initial V_{oc} than those with lower initial V_{oc}.

Based on the concept of the two-diode model, most of the kinetic results are understandable. First, the cells with an initial V_{oc} around 0.6 - 0.8 V (depending on the cell structure and the light soaking condition) has a wider spread between the two curves of Fig. 19 (b), which means that any change in the microcrystalline volume fraction or forward current density would produce a large $\triangle V_{oc}$. Experimentally, the largest light-induced V_{oc} increase appears at around 0.75 V with a bell-shaped curve on the $\triangle V_{oc}$ versus the initial V_{oc} plot. Therefore, the increase rate for the cells with intermediate initial V_{oc} is higher than those with

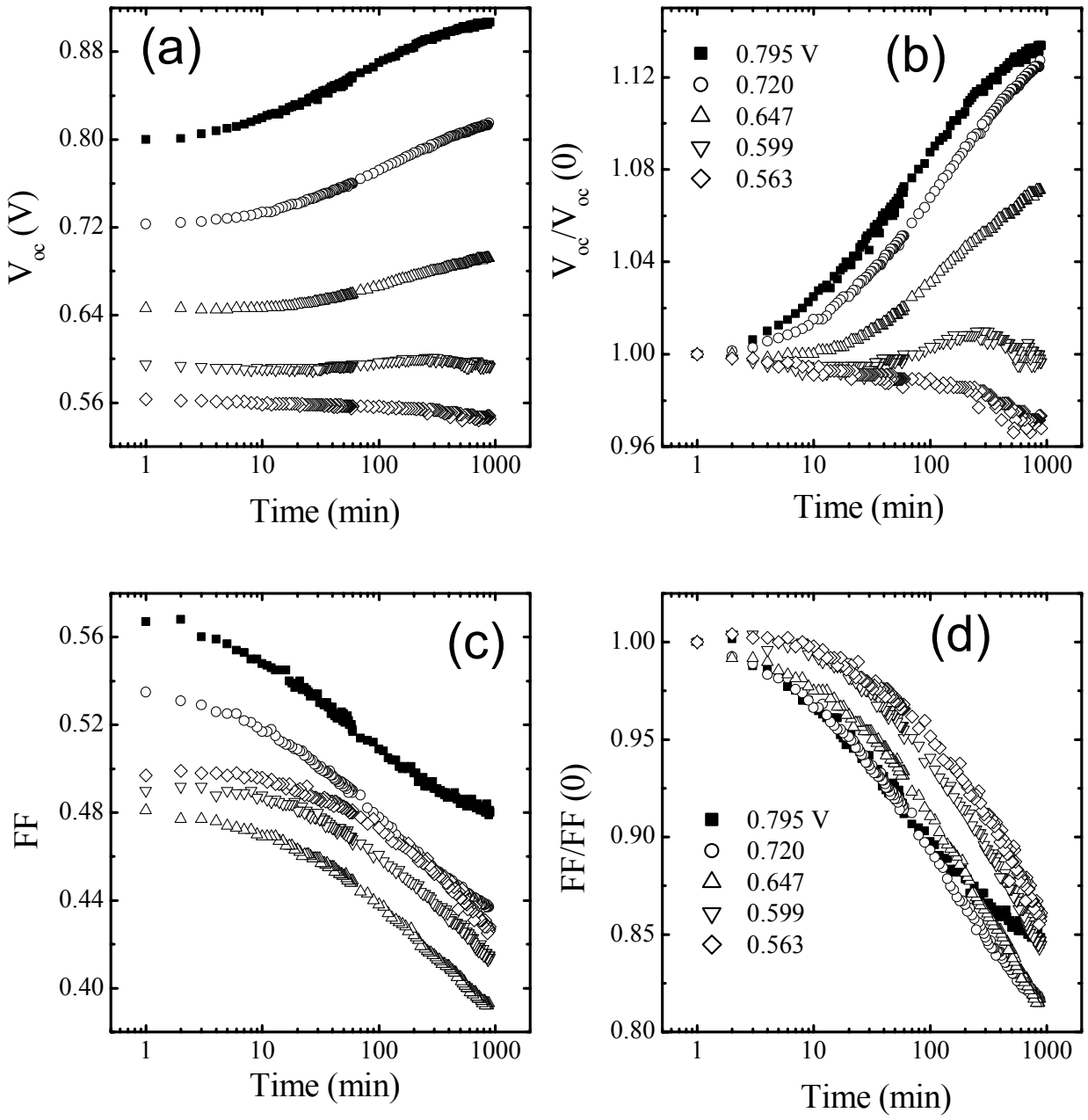

Figure 24. Kinetics of V_{oc} and FF for the cells with various initial V_{oc} on the μc-Si side: (a) V_{oc}, (b) normalized V_{oc}, (c) FF, and (d) normalized FF.

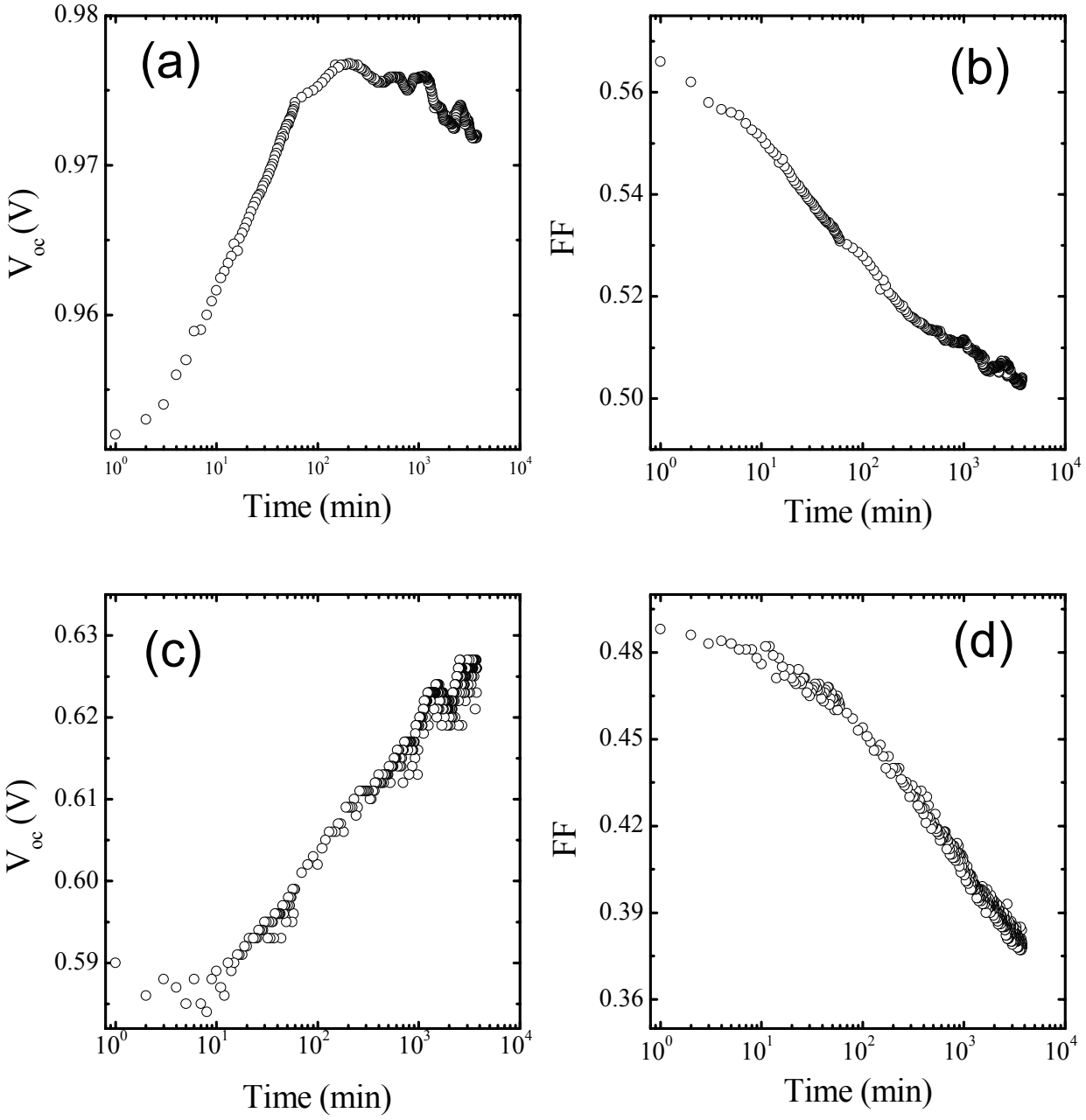

Figure 25. Kinetics of V_{oc} and FF of the cells with an initial V_{oc} of 0.952 V [(a), (b)] and 0.590 V [(c), (d)] for 67 hour-light soaking.

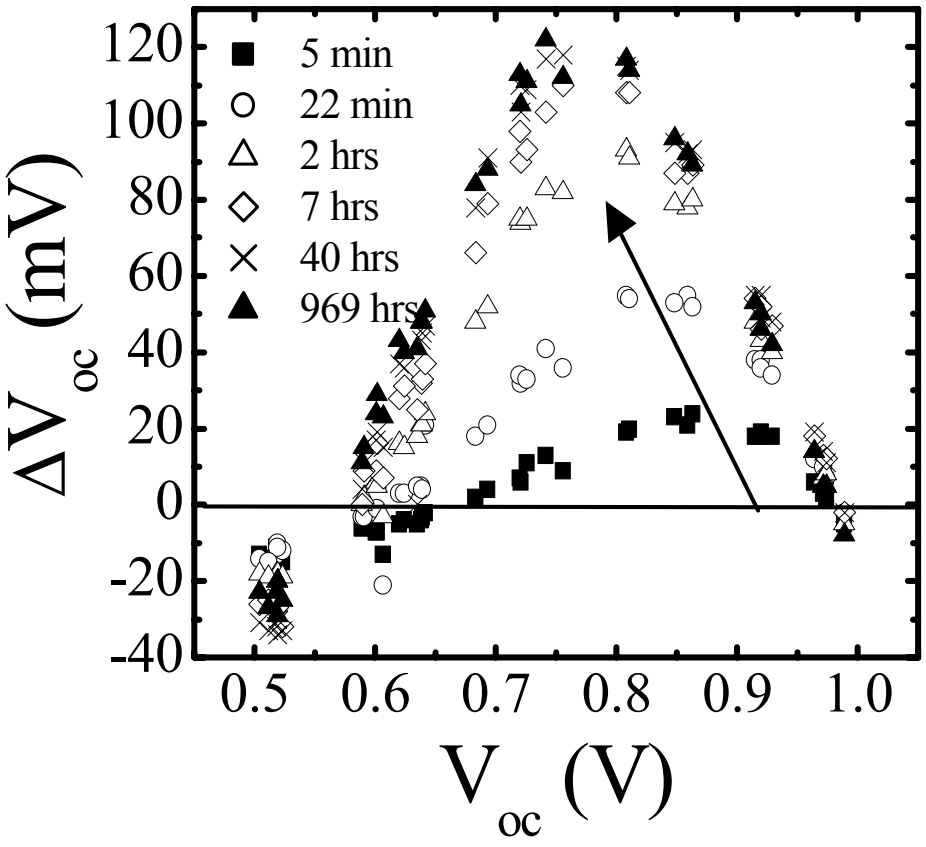

Figure 26. ΔV_{oc} as a function of initial V_{oc} for different exposure times. The arrow indicates the shift in the peak position.

smaller or larger initial V_{oc}. In addition, the cells with low initial V_{oc} (~ 0.6 V) would move towards the unstable region, but the cells with high initial V_{oc} would move out of the unstable region. Consequently, on the average, the cells with initial $V_{oc} < 0.8$ V show a smaller increase rate and a slower tendency to saturate than cells with initial $V_{oc} > 0.8$ V, as shown in Figs. 23 and 24. As a result, the maximum on the $\triangle V_{oc}$ versus initial V_{oc} plot shifts to a lower initial V_{oc} as the light soaking time increases (see Fig. 26). The saturation or decrease of V_{oc} after a period of light soaking for the cells with a high initial V_{oc} could be explained as follows. The decrease of forward current for the μc-Si:H cell due to a reduction of forward current density or reduction of microcrystalline volume fraction is offset by the reduction of current from the a-Si:H, due to the Staebler-Wronski effect that is more pronounced at voltages around 0.85 eV for an a-Si:H cell. We should point out that Fig. 19 is just an illustration. The choices of J-V curves for a-Si:H and μc-Si:H diodes are somewhat arbitrary. In a real mixed-phase cell, the characteristics of the equivalent a-Si:H and μc-Si:H are unknown. Therefore, quantitative predictions of the amount of light-induced V_{oc} increase, and kinetic behavior cannot be made.

Previously, we have reported that the origin of light-induced V_{oc} increase is the same as Staebler-Wronski effect. Recombination of photo-generated carriers produces metastable defects in both μc-Si:H (may be at grain boundary region) and a-Si:H phases. Therefore, it is not difficult to understand why the FF for all the cells decreases with light-soaking time.

5.5. Summary

Light-induced V_{oc} in mixed-phase solar cells has been systemically studied. A two-diode equivalent circuit model has been proposed to explain the change of initial V_{oc} with increasing microcrystalline volume fraction. The model is consistent with most experimental results. A new experiment with different buffers provides additional supporting evidence for the model. We believe that the light-induced microcrystalline volume fraction change (if any) and the reduction of forward current in the microcrystalline region are the two causes of the light-induced V_{oc} increase. At this moment, we cannot distinguish which effect has the main contribution. Kinetics of light-induced V_{oc} in the mixed-phase solar cells has been measured. The kinetics behaviors are different for cells with different initial V_{oc} and also can be explained using the two-diode equivalent circuit model.

Section 6

Status of Amorphous Silicon Alloy Component and Multijunction Cells and Modules Deposited in a Large-Area Reactor

6.1. Introduction

In the past, the best cells in R&D were fabricated by optimizing each deposition parameter independently. Some of these parameters are incompatible with the new 30MW/year roll-to-roll production machine. For example, the deposition rate for the intrinsic layer for the R&D case was lower than that of production. There was a disconnect between the R&D technology and manufacturing technology. In the last couple of years, an attempt has been made to bridge this gap. The manufacturing operation continuously "learns" from the R&D experience and changes are implemented wherever possible in order to improve cell efficiency. Conversely, a focused effort has been initiated in R&D to embrace the limitations of the deposition parameters in production. One objective under the current NREL contract is to expand this approach to encompass standardization of deposition hardware for both R&D and manufacturing. One important issue that is being addressed is the design of the RF cathode assembly for the deposition of the *n*, *i*, and *p* layers. The ultimate objective is to do research in improving cell quality in R&D using similar deposition hardware and parameters as to those in the production machine. Any advances made in R&D can then be translated relatively easily to production. With this in mind, the cathode assembly in all three deposition chambers of the large-area "2B machine" in R&D has been modified to mimic the 30MW/year production machine. The new cathodes are referred to as "fountain cathodes".

In R&D, the best triple-junction cells employ a-SiGe intrinsic layers (for the middle and bottom cells) fabricated using Si_2H_6/GeH_4 gas flow. The rationale is that Si_2H_6 and GeH_4 have similar dissociation rates that in turn lead to a similar Si/Ge ratio in the films over large gas flow distances. Replacement of the Si_2H_6/GeH_4 gas mixture with SiH_4/GeH_4 will lead to substantial cost savings. The challenge is to deposit cells with good quality with no gas depletion using the new gas mixture. The deposition parameters for best cell performance are dependent on the cathode hardware geometry. Preliminary work on the optimization of middle and bottom cells fabricated using SiH_4/GeH_4 gas mixture using the new RF cathode assembly has been done.

A prerequisite to fabricating large area high efficiency modules is to optimize the performance and the uniformity of smaller area cells. This approach enables the diagnosis and analysis of the devices at both the cell and module levels. Evaluation of the small-area (total area = 0.268 cm^2, active area = 0.25 cm^2) cells using I-V and Q measurements provide information about the basic device efficiency without the complications of electrical and optical losses associated with modules. It also enables the evaluation and optimization of the device at the component cell level.

6.2. Experimental

Stainless steel substrate with no back reflector has been used for depositing various layers for thickness uniformity studies. In order to quantify the thickness uniformity of various layers, the thickness of each layer has been measured at 26 locations over an 11" X 11" area using

Rudolph Thickness Monitor. The measurements have been made for layers both before and after the cathode change. Two independent quantities have been used for this analysis:

- hi-lo (%) = (maximum thickness – minimum thickness) / maximum thickness and
- coefficient of variation of thickness distribution: CV (%) = standard deviation/average.

For component cell studies, stainless steel substrate with no back reflector is used for fabricating the top and middle cells. For the bottom cell, a textured Al/ZnO back reflector layer on stainless steel substrate is used for device fabrication. The deposition of the back reflector and a-Si:H and a-SiGe:H layers are made over an area of ~1 sq. ft. Conventional RF glow discharge technique is used for the semiconductor deposition. The completed large-area device is cut into several ~2"x2" pieces representing a 10"x10" area. The transparent conducting layer (TCO) is deposited through an evaporation mask to yield an array of devices of total area 0.268 cm^2. These devices are used for I-V and Q measurements.

6.3. Layer thickness uniformity

Figure 27 shows hi-lo uniformity of various layers over an 11" X 11" area. The fountain cathode exhibits significantly improved hi-lo uniformity, from ~55% to ~23%. Figure 28 shows uniformity distribution based on CV. The fountain cathode exhibits superior CV uniformity, from ~22% to ~8%. Table VI summarizes the average uniformity data of individual layers using both cathodes. Note that these are the average of all the values of hi-lo and CV uniformity as obtained from Figs. 27 and 28. Clearly, the average uniformity values are superior for the fountain cathode.

Table VI. Average uniformity data of individual layers for flat and fountain cathodes.

Layer	Cathode	Hi - Lo (11 x 11")	CV (11 x 11")
I1	Standard	54%	22.5%
	Fountain	**24%**	**10%**
I2	Standard	46%	17.9%
	Fountain	**23%**	**8%**
I3	Standard	55%	21.3%
	Fountain	**23%**	**8.5%**

6.4. Design Of Experiments (DOE)

In order to improve the thickness uniformity we have undertaken to use the DOE technique. We have carried out a series of experiments using Taguchi Robust Design of Experiments (orthogonal arrays). Preliminary results indicate that there is scope of further improvement in the thickness uniformity distribution. In fact, even within the first DOE, some layers already provided significantly better uniformity than what we had ever achieved before. For example, the best uniformity we had ever realized for I1 layer was 10% (based on CV); in the DOE, one of the depositions reduced the thickness distribution to 5.9%.

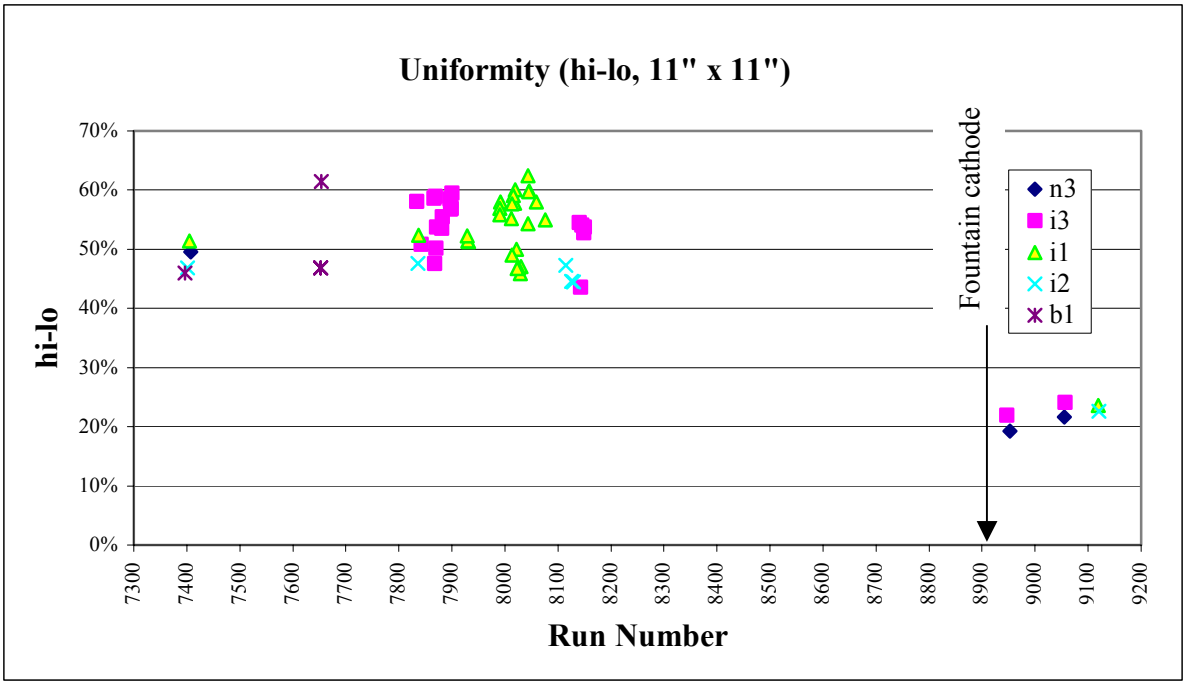

Figure 27. hi-lo uniformity over 11” x 11” before and after fountain cathode.

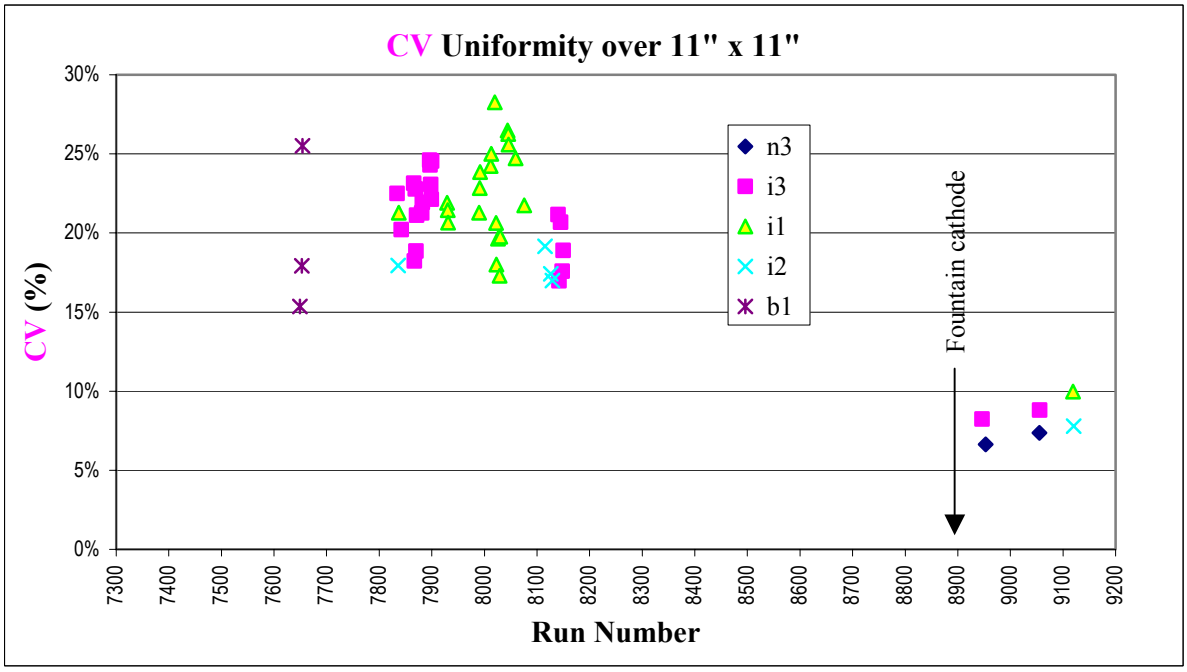

Figure 28. CV uniformity over 11” x 11” before and after fountain cathode.

6.5. Uniformity of component cell performance

6.5.1. Top Cell on Stainless Steel Substrate

Seven ~2"x2" pieces of the top cell representing the large-area 10"x10" stainless steel substrate with no back reflector, were selected. The I-V characteristics were measured using AM1.5 illumination. The initial performance of devices and their average values are listed in Table VII. Each value in the table represents the average of two 0.268 cm^2 devices on that substrate. The best average total-area efficiency is ~6.4% for sample RLC1 while the average of all cells on the seven pieces is 6.16%. The standard deviation and coefficient of variation of the seven samples are also listed at the bottom of Table VII. The standard deviation is 0.24 and the coefficient of variation is 3.8%.

Table VII. Initial Performance of Top Cells Measured over 10" X 10" Deposition Area.

Sample	Substrate	Area	Source	Efficiency	J_{sc}	V_{oc}	FF	R_s
2B9117		(cm^2)		(%)	(mA/cm^2)	(V)		Ohm
LN	SS	0.268	1.5	5.75	7.63	1.003	0.751	6.4
LLC1	SS	0.268	1.5	6.36	8.55	1.004	0.741	7.0
LS	SS	0.268	1.5	6.25	8.47	0.999	0.738	8.3
RN	SS	0.268	1.5	6.06	8.14	1.005	0.741	8.5
RLC1	SS	0.268	1.5	6.42	8.62	1.006	0.742	7.6
RS	SS	0.268	1.5	6.29	8.45	1.006	0.741	8.1
LC1	SS	0.268	1.5	6.02	8.42	0.997	0.717	10.2
Average				**6.16**	**8.33**	**1.003**	**0.738**	**8.0**
Standard Deviation				**0.24**	**0.34**	**0.003**	**0.011**	**1.21**
Coefficient of Variation				**3.83%**	**4.10%**	**0.34%**	**1.42%**	**15.13%**

6.5.2. Middle Cell on Stainless Steel Substrate

Similar work has been done on the middle cell on stainless steel substrate with no back reflector. Nine representative ~2"x2" pieces with 0.268 cm^2 total-area devices were prepared. The initial performance of the devices was measured under AM1.5 illumination using a λ>530 nm cut-on filter, as listed in Table VIII. The average values of total-area P_{max} at λ>530 nm of the nine substrates are in the range of 3.11-3.45 mW/cm^2. Sample LLC1 exhibits the best performance. The average performance is 3.2 mW/cm^2. The standard deviation and coefficient of variation of the nine samples are also listed at the bottom of Table VIII. The standard deviation is 0.10 and the coefficient of variation is ~3.0%.

6.5.3. Bottom cell on Al/ZnO back reflector

For the bottom cell, an Al/ZnO back reflector substrate has been used. Seven representative ~2"x2" pieces with 0.268 cm^2 total-area devices were prepared. The initial performance of the devices was measured under AM1.5 illumination using a λ>610 nm cut-on filter, as listed in Table IX. The average values of total-area P_{max} at λ>610 nm of the seven substrates are in the range of 2.83-3.08 mW/cm^2. Sample LN exhibits the best performance.

Table VIII. Initial Performance of Middle Cells Measured over 10" X 10" Deposition Area.

Sample	Substrate	Area	Source	P_{max}	J_{sc}	V_{oc}	FF	R_s
2B9179		(cm^2)	(nm)	(mW/cm^2)	(mA/cm^2)	(V)		Ohm
LN	SS	0.268	530	3.28	6.99	0.690	0.685	9.7
LLC1	SS	0.268	530	3.45	7.42	0.678	0.687	8.4
LS	SS	0.268	530	3.23	7.29	0.673	0.658	9.3
RN	SS	0.268	530	3.18	7.40	0.668	0.644	11.1
RLC1	SS	0.268	530	3.25	7.19	0.674	0.671	9.7
RS	SS	0.268	530	3.24	7.31	0.673	0.659	11.2
N	SS	0.268	530	3.17	6.88	0.680	0.677	8.7
LC1	SS	0.268	530	3.19	6.75	0.683	0.691	8.9
S	SS	0.268	530	3.11	6.62	0.683	0.688	8.9
Average				**3.23**	**7.10**	**0.678**	**0.673**	**9.5**
Standard Deviation				**0.10**	**0.29**	**0.01**	**0.02**	**1.01**
Coefficient of Variation				**2.99%**	**4.12%**	**0.99%**	**2.45%**	**10.56%**

The average performance is 3.0 mW/cm^2. The standard deviation and coefficient of variation of the seven samples are also listed at the bottom of Table IX. The standard deviation is 0.09 and the coefficient of variation is ~3.0%.

Table IX. Initial Performance of Bottom Cells Measured over 10" X 10" Deposition Area.

Sample	Substrate	Area	Source	P_{max}	J_{sc}	V_{oc}	FF	R_s
2B9170		(cm^2)	(nm)	(mW/cm^2)	(mA/cm^2)	(V)		Ohm
LN	SS	0.268	610	3.08	8.14	0.595	0.636	10.5
LLC1	SS	0.268	610	3.06	8.82	0.573	0.606	10.6
LS	SS	0.268	610	2.97	7.85	0.591	0.639	10.1
RN	SS	0.268	610	3.00	7.47	0.613	0.656	10.7
RLC1	SS	0.268	610	2.94	7.53	0.604	0.647	10.2
RS	SS	0.268	610	3.05	7.83	0.606	0.643	11.6
LC1	SS	0.268	610	2.83	8.29	0.568	0.600	10.1
Average				2.99	7.99	0.593	0.632	10.5
Standard Deviation				0.09	0.47	0.02	0.02	0.53
Coefficient of Variation				2.97%	5.91%	2.86%	3.35%	4.98%

6.6. Summary

The 2B machine has been modified to accommodate new RF fountain cathodes. The thickness uniformity of various layers is superior to that obtained with the earlier cathodes. Component top, middle, and bottom single-junction cells have been fabricated and the uniformity of device performance has been investigated.

Section 7

Future Work

We have made significant progress in different aspects of the program during the first year. We will continue our efforts to accomplish the milestones of the next year. The work plan for the coming year is summarized below.

7.1. Thickness dependence of μc-Si:H films and devices

We will continue to work on the optimization of μc-Si:H solar cell and use μc-Si:H solar cell as the bottom cell in a multi-junction structure. Last year, we achieved an initial efficiency ~13.0% using RF at a low rate. Compared to the published results of Kaneka and Canon, our μc-Si:H cell has low current density. Normally, our μc-Si:H solar cells exhibit J_{sc} ~ 22 to 24 mA/cm^2, which is significantly lower than Kaneka's result of 27-30 mA/cm^2. We can increase J_{sc} by increasing the intrinsic layer to >2 μm, but the V_{oc} and FF decrease dramatically. Before we can improve the cell efficiency further, we need to understand what causes the decreases of V_{oc} and FF with increase of cell thickness. We have identified two potential problems listed below.

1. Collision of microcrystallites

It has been shown that microcrystalites grow in columnar shapes perpendicular to the growing surface. When a cell is deposited on a textured substrate, two adjacent microcrystallites will meet when the film attains a certain thickness. The collision of microcrystallites causes high defect density and low cell performance. We will investigate if the collision of microcrystallites is a major problem. If it is, we need to optimize the Ag/ZnO back reflector to reduce the texture, or keep a similar texture but change the shape/size of the micro-features of the back reflector to avoid microcrystalline collision.

2. Microcrystalline evolution with film thickness

Microcrystalline volume fraction increases with film thickness when hydrogen dilution is constant. A high microcrystalline volume fraction may lead to high density of microvoid and microcracks. The ensuing high defect density leads to poor cell performance. We will explore ramping the deposition parameters, such as hydrogen dilution in order to achieve uniform material property throughout the thickness of the film.

7.2. Optimization a-SiGe:H middle cells for a-Si:H/a-SiGe:H/a-SiGe:H and a-Si:H/a-SiGe:H/μc-Si:H triple-junction cells

μc-Si:H solar cells has attracted considerable attention due to low light-induced degradation and elimination of GeH_4 in the PECVD process. However, the a-Si:H/a-SiGe:H/a-SiGe triple-junction cell structure exhibits the best stable efficiency to date. We believe that

there is scope for improving the cell performance of a-SiGe:H solar cell further. We propose to continue our effort in the optimization of such cells and identified two specific areas.

1. Develop a-SiGe:H middle cell for a-Si:H/a-SiGe:H/μc-Si:H triple-junction structure

a-Si:H/μc-Si:H double-junction cell has shown respectable efficiency. In order to improve the efficiency further, we need to focus on increasing the J_{sc} of the device. One way to attain high J_{sc} is to increase the thickness of the a-Si:H top cell. However, this approach is beset with the problem of poor stability. We believe that a-Si:H/a-SiGe:H/μc-Si:H triple-junction structure has a better chance of attaining high stable efficiency. For this purpose, we shall optimize the a-SiGe:H recipe for compatibility with the μc-Si:H bottom cell.

2. Explore new regime for a-SiGe:H deposition

We will investigate the use of narrower band gap a-SiGe:H films to obtain higher stable multi-junction cell efficiency. It has been reported that defect density increases with Ge content in a-SiGe:H films in the Si-rich regime due to the heavier Ge radicals and higher chemical disorder. We will embark on a Ge-rich regime in a-SiGe:H films and explore the possibility of obtaining a material with lower defect density and superior cell efficiency.

7.3. Optimization large-area deposition

We will continue to optimize thickness and cell performance uniformity using the new fountain cathodes. We will start deposition of triple-junction cells and do stability studies. Once we attain high device efficiency, we will make large area modules.